POLITECNICO DI TORINO

Master's Degree in Green Building Engineering

Master's Thesis

Performance Evaluation and Geographical Assessment of Grid-Connected Photovoltaic Systems in Residential Buildings Across the Czech Republic: A Multi-Province Simulation, Sensitivity Analysis, and Spatial Optimization Study

Supervisors:

Prof. CAPPELLUTI FEDERICA (DET)

Prof. WACLAWEK STANISLAW (External Supervisor)

Candidate:

AMIRHOSSEIN AHMADI

July 2026

Table of Contents

Performance Evaluation and Geographical Assessment of Grid-Connected Photovoltaic Systems in Residential Buildings Across the Czech Republic: A Multi-Province Simulation, Sensitivity Analysis, and Spatial Optimization Study

Abstract

The accelerating deployment of residential solar photovoltaic (PV) systems across Europe, driven by the recast Energy Performance of Buildings Directive (EPBD, 2024/1275/EU) mandate for zero-emission buildings by 2030, demands spatially resolved performance benchmarks at the provincial scale. Generic European-level models lack the resolution required for building-level design and investment decisions, and province-specific performance data for Central European climates remain scarce in the peer-reviewed literature.

To the authors' knowledge, no prior study has presented a systematic, multi-province performance evaluation of a standardised 12 kWp grid-connected rooftop PV system across all 13 administrative provinces of the Czech Republic. Meteorological inputs were obtained from Meteonorm 8.1 and integrated into PVsyst v7 simulation software. The system configuration comprises JinkoSolar 435 Wp N-type monocrystalline Tunnel Oxide Passivated Contact (TOPCon) modules (28 modules in two independent strings of 14) paired with a Huawei 12 kW dual-MPPT inverter, installed on a representative Czech single-family rooftop of 56 m^2. Performance indicators - final yield (Y_f), performance ratio (PR), annual energy delivered to grid (E_{grid}), and system losses - are defined and reported in accordance with IEC 61724-1:2017.

The province-specific optimal tilt angle ranges from 38 to 42 degrees, systematically 8–12 degrees below the geographic latitude of 49–51 degrees N, with Prague showing the largest deviation (~12°) due to its comparatively low optimal tilt of 38° relative to its 50.1°N latitude - a finding explained by the high diffuse radiation fraction and summer-dominant energy balance of Czech temperate climates, with practical implications for residential building design. Annual Y_f ranges from 2.96 kWh/kWp/day (Prague) to 3.27 kWh/kWp/day (Ceske Budejovice), and PR lies within 89.1%-89.7% - among the highest values reported internationally, confirming that Central European climates are exceptionally favourable for residential PV efficiency. Total annual E_{grid} varies from 13,169 kWh to 14,533 kWh, corresponding to a nZEB energy coverage of 40-58% of the primary energy consumption of a typical Czech dwelling.

A Monte Carlo simulation framework (N = 1000 realisations per province, implemented in MATLAB 2019b) combined with one-at-a-time sensitivity analysis identifies plane-of-array irradiance as the dominant performance uncertainty driver (sensitivity index 0.85-0.95), confirming that meteorological variability - not system design parameters - constitutes the primary source of yield risk. Hradec Kralove, Usti nad Labem, and Jihlava exhibit the highest sensitivity to climatic uncertainty; Prague presents the most stable performance profile with the lowest Value-at-Risk at the 5% quantile.

Principal component analysis (PCA) reduces the provincial performance matrix to two dominant components explaining 62.5% of total variance (a third component contributes a further 16.0%), interpreted as a solar resource intensity axis and a thermal efficiency axis. K-means clustering reveals a markedly asymmetric structure: two broadly similar province groups differing by only 1.7% in mean Y_f (a 5-province higher-performing group and a 7-province group), and Prague as a singular outlier at Y_f = 2.96 kWh/kWp/day, 7.6-9.5% below both groups - indicating that performance disparities are driven primarily by Prague's distinct urban microclimate rather than a broader regional divide. The aggregate provincial portfolio exhibits a coefficient of variation of 2.8%, below the mean provincial value of 4.3-4.5%, demonstrating the systemic risk-reduction benefit of geographic diversification.

These findings contribute a technically rigorous, spatially resolved, and probabilistically bounded performance dataset for Czech residential PV systems, directly supporting evidence-based nZEB building design and region-differentiated renewable energy policy aligned with EU EPBD compliance requirements.

Keywords: *Photovoltaic (PV) systems; residential buildings; grid-connected systems; performance ratio; final yield; optimal tilt angle; Monte Carlo simulation; sensitivity analysis; PVsyst; Meteonorm; nearly zero-energy buildings (nZEB); spatial analysis; principal component analysis; Czech Republic; green building engineering*

ACKNOWLEDGMENTS

I would like to express my sincere gratitude to my supervisors, Prof. Federica Cappelluti and Prof. Stanislaw Waclawek, for their guidance, constructive feedback, and continued support throughout the development of this thesis. Their expertise and availability were invaluable in shaping both the research direction and the quality of the final work.

I am grateful to Politecnico di Torino and the Master's programme in Green Building Engineering for providing the academic environment and resources that made this research possible. I also wish to acknowledge the support of the institutions and research community in the Czech Republic whose publicly available data, solar resource maps, and policy documentation formed an essential part of the evidence base for this study.

I would like to thank my colleagues and fellow students for the stimulating discussions, shared knowledge, and encouragement throughout this programme. Their collegiality made the experience of graduate study both more productive and more enjoyable.

Finally, my deepest gratitude goes to my family, whose unconditional support, patience, and encouragement have been the foundation of everything I have accomplished. This work is dedicated to them.

Contents

List of Figures

List of Tables

Chapter 1: Introduction

1.1 Background and Motivation

The global energy system is undergoing a structural shift driven by climate policy, declining technology costs, and energy security imperatives. Solar photovoltaic (PV) technology has emerged as the leading instrument of this transition. According to the IEA-PVPS Snapshot of Global PV Markets 2024, cumulative global PV capacity reached 1.6 TW in 2023, with 446 GW of new capacity commissioned in a single year [1]. Figure 1.1 shows the rapid growth of global renewable power capacity between 2013 and 2030. Total renewable additions are projected to increase from about 1 000 GW in 2013–2018 to nearly 4 600 GW in 2025–2030. Solar PV is expected to dominate this growth, increasing its share from around 45% to almost 80% by 2030 due to declining costs, faster deployment, and strong policy support. The figure also indicates that renewable energy deployment is accelerating globally, despite ongoing challenges related to grid integration, financing, and infrastructure development [2]. These figures indicate a structural shift in the electricity generation mix, with PV emerging as the largest contributor to new capacity additions.

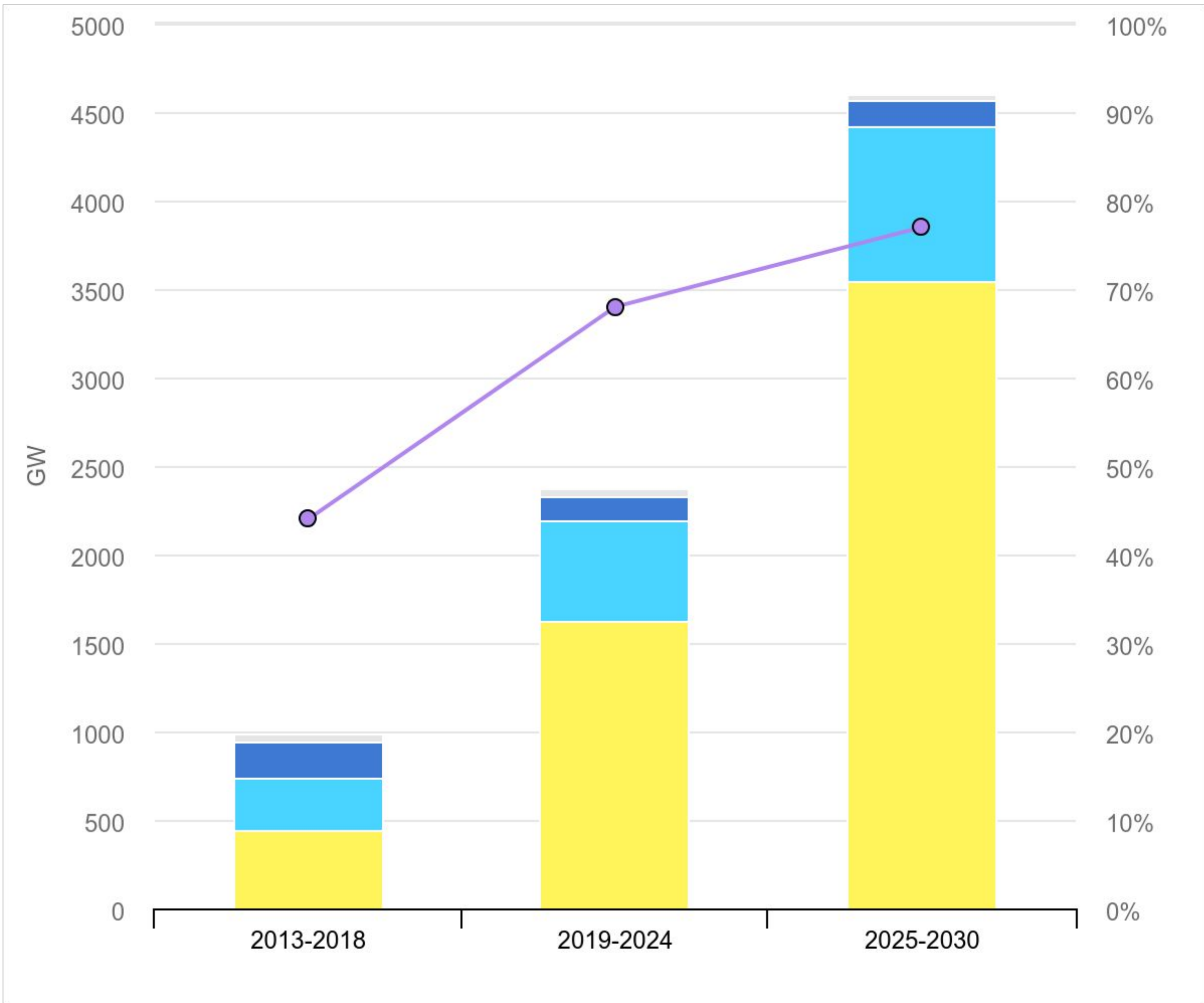

Figure Introduction.1. Global renewable power capacity additions by technology segment and the share of solar PV in total renewable growth for the periods 2013–2018, 2019–2024, and 2025–2030 (main case scenario). Solar PV is projected to dominate renewable capacity expansion, accounting for nearly 80% of total additions by 2030 [2]

Within this global context, the residential building sector occupies a critical position. Buildings are responsible for approximately 40% of total energy consumption and 36% of CO_2 emissions in the European Union [3]. The recast Energy Performance of Buildings Directive (EPBD, Directive 2024/1275/EU) mandates that all new buildings must achieve zero-emission building (ZEB) standards by 2030, with public buildings required to comply by 2028 [3]. Rooftop PV systems on residential buildings are among the most direct technical pathways to meeting these targets, contributing to reduced grid demand, lower operating energy costs, and improved energy autonomy. Bódis et al. [4] demonstrated that EU rooftops could theoretically produce 680 TWh of solar electricity annually, covering 24.4% of the EU's electricity consumption at the time of the study.

Despite this strategic importance, a fundamental gap persists: the technical performance of residential rooftop PV systems varies substantially by geography, climate, and local environmental conditions [5]. Generic European-scale assessments cannot provide the provincial-level resolution needed by building designers, energy engineers, or policymakers making investment and design decisions at the building or municipal scale. This gap is particularly acute in Central European countries such as the Czech Republic, where PV expansion has accelerated dramatically from 2,460 MWp in 2022 to approximately 5,160 MWp by end of 2025, driven largely by residential installations supported by the New Green Savings Program [6], yet spatially resolved performance data at the provincial level remains scarce in peer-reviewed literature.

1.2 Research Context: PV in the Czech Republic

The Czech Republic presents a particularly instructive case study. Located between latitudes 49 and 51 degrees N, with a moderate continental climate characterized by distinct seasonal solar irradiance variation, the country has 13 administrative provinces with different geographic and climatic profiles in terms of altitude, cloud cover, ambient temperature, and diffuse radiation fractions. Average annual global horizontal irradiance (GHI) across the country is approximately 949-1168 kWh/m^2 (Figure 1.2), but provincial values diverge depending on local topography and atmospheric conditions [7].

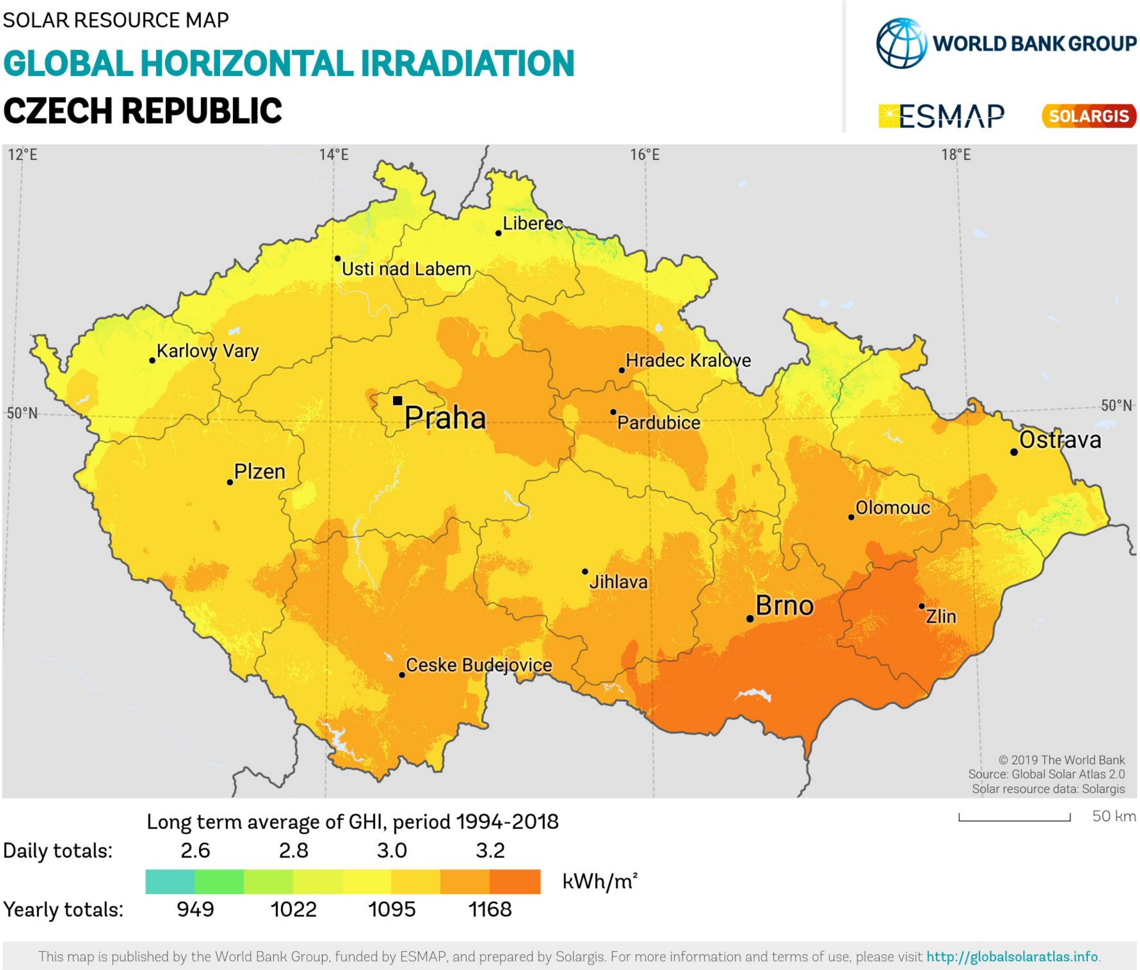

Figure Introduction.2. Global Horizontal Irradiation (GHI) distribution map of the Czech Republic based on long-term average solar resource data for the period 1994–2018. The map illustrates spatial variations in solar irradiation, with higher solar potential observed mainly in the southern and southeastern regions of the country.

The country's PV policy history further justifies detailed performance analysis. After a feed-in tariff collapse between 2010 and 2013, Czech PV deployment stagnated for over a decade. The policy framework was rebuilt through EU directive transposition rather than domestic political initiative, as documented by Tanil and Jurek [8], who found that renewable energy policy in the Czech Republic has been primarily a top-down, EU-compliance-driven process with limited internal political ownership. This context matters for performance assessment: systems designed and installed under policy uncertainty, or without geographically tailored design standards, may operate sub-optimally. Understanding province-specific performance variation is therefore not merely an academic exercise but a prerequisite for evidence-based policy and building design practice.

Household-level adoption data reinforces the relevance of this work. Makesova et al. [9] found that 83% of Czech residential PV adopters cited financial subsidies and 61% cited environmental benefits as primary motivators. However, neither subsidy design nor consumer decision-making currently incorporates province-specific yield and loss data in a systematic way. A rigorous, multi-province performance dataset which this thesis provides is a prerequisite for such integration.

1.3 Problem Statement

Existing studies on Czech PV performance are predominantly single-location or single-system assessments. Broader comparative analyses using tools such as PVGIS or satellite-derived irradiance datasets provide pan-European coverage but at spatial resolutions (typically 1-5 km grid cells) that are insufficient for province-level or building-level decision-making [4]. Furthermore, most published studies report deterministic simulation outputs without uncertainty quantification, leaving the question unanswered of how sensitive performance metrics are to variability in key input parameters such as irradiance, temperature, and system losses.

Three specific gaps motivate this thesis:

1. A systematic performance analysis of a standardized residential photovoltaic system across the 13 Czech provinces, based on PVsyst simulations, remains absent from the existing peer-reviewed literature.

2. Monte Carlo-based uncertainty quantification and sensitivity analysis have not been applied to characterize the stochastic behavior of residential PV performance in a Central European multi-province context.

3. Spatial and multivariate statistical analysis linking PV performance metrics to geographic and climatic variables across Czech provinces using methods such as PCA and K-means clustering has not been conducted at this scale.

PVsyst v7 is selected as the simulation platform to address Gap 1 because it implements the one-diode model with irradiance-dependent shunt resistance [10], produces IEC 61724-1:2017 compliant outputs natively, and has been validated against field measurements with deviations below 3% for fixed-tilt systems in temperate climates [11]. Alternative tools such as PVGIS provide pan-European coverage but operate on coarser spatial grids (1–5 km) with deterministic outputs and no Monte Carlo capability, making them unsuitable for the province-resolved probabilistic analysis required here.

1.4 Research Objectives

This thesis addresses the above gaps through the following specific objectives:

1. To simulate and evaluate the annual performance of a standardized 12 kWp grid-connected rooftop PV system across all 13 Czech provinces using PVsyst v7, with meteorological data from Meteonorm 8.1, reporting final yield (Y_f), performance ratio (PR), energy delivered to grid (E_{grid}), and system losses in accordance with IEC 61724-1:2017 [12].

2. To determine the optimal panel tilt angle for each province and quantify the sensitivity of annual energy yield to tilt deviations, distinguishing summer and winter performance characteristics.

3. To quantify the uncertainty in key performance indicators through a Monte Carlo simulation framework and identify the most influential input parameters through one-at-a-time (OAT) sensitivity analysis, following the methodology of Saltelli et al. [13].

4. To characterize the spatial distribution of PV performance across the Czech Republic through GIS-based mapping and to identify province clusters with shared performance characteristics using PCA, K-means, and hierarchical clustering.

5. To contextualize the performance findings within the EU EPBD framework and Czech national energy policy, identifying implications for building design practice and region-differentiated policy instruments.

1.5 Scope and Limitations

The study is bound by the following scope of decisions, each of which carries implications that must be acknowledged explicitly.

System standardization: A single system configuration (12 kWp, JinkoSolar 435 Wp modules, Huawei 12 kW inverter, fixed tilt, south-facing) is applied uniformly across all provinces. This allows direct inter-province performance comparison but does not capture the effect of system size variation, module technology choice, or tracking systems. The 12 kWp capacity and 56 m^2 rooftop area correspond to a representative Czech single-family dwelling and are consistent with the average domestic installation size recorded by the Czech Solar Association in 2025 (11.4 kWp) [6].

Simulation fidelity: PVsyst v7 is used as the primary simulation platform. Its one-diode model for PV module characterization has been validated against measured field data with deviations typically below 3% for fixed-tilt systems under temperate conditions, as confirmed by Ahmad et al. [14]. Meteorological inputs from Meteonorm 8.1 represent long-term typical-year averages; year-to-year climate variability is addressed through Monte Carlo sampling rather than multi-year measured data.

Economic and lifecycle scope exclusion: No techno-economic analysis (LCOE, NPV, payback period) or life-cycle assessment (LCA) is conducted. This is an acknowledged limitation and is explicitly identified as a priority for future research. The exclusion is deliberate: introducing economic parameters would require province-specific electricity tariff data, subsidy structures, and financing assumptions that are outside the defined scope of this green building performance study. The thesis is a technical performance study, not a feasibility assessment.

Shading and 3D environment: Simulations assume no near-shading from surrounding structures or vegetation. Real installations may experience shading losses beyond those captured in the model. Three-dimensional shading analysis using actual building geometry is identified as a recommended extension.

1.6 Thesis Structure

The remainder of this thesis is organized as follows. Chapter 2 establishes the theoretical background, covering PV cell physics, performance indicator definitions per IEC 61724-1:2017, tilt angle optimization theory, and the regulatory context of nZEB standards in Europe.

Chapter 3 describes the methodology, including the case study configuration, PVsyst simulation workflow, Monte Carlo framework, and statistical analysis methods. Chapter 4 presents and discusses the results across five subsections: tilt optimization, weather and irradiance analysis, system loss decomposition, normalized performance coefficients and Monte Carlo sensitivity, and spatial and multivariate statistical analysis. Chapter 5 states the conclusions and recommendations for future research.

Chapter 2: Theoretical Background

2.1 Photovoltaic Effect and Solar Cell Physics

2.1.1 The Photovoltaic Effect

The photovoltaic effect the direct conversion of light into electrical energy was first observed by Becquerel in 1839 [15] and later formalized through quantum theory by Einstein in 1905 [16]. In a crystalline silicon solar cell, photons with energy greater than the bandgap of silicon (Eg = 1.12 eV at 300 K) are absorbed and generate electron-hole pairs through the inner photoelectric effect [17]. These charge carriers are separated by the built-in electric field at the p-n junction, producing a photocurrent. The theoretical framework for p-n junction behavior, including the ideal diode equation, was established by Shockley [18], whose single-exponential model remains the basis of all standard PV simulation tools, including PVsyst.

2.1.2 The One-Diode Model

The electrical behavior of a PV cell is most accurately described by the one-diode equivalent circuit model, comprising a current source (I_{ph}), an ideal diode, a series resistance (R_s), and a shunt resistance (R_{sh}). The terminal current-voltage (I-V) relationship is given by [19], [20]:

(Eq. 2.1)

where I_0 is the dark saturation current, n is the diode ideality factor (1 for ideal diffusion-dominated recombination, 2 for space-charge recombination), and $V_t = kT/q$ is the thermal voltage (approximately 25.7 mV at 300 K). Mermoud and Lejeune [10] extended this model within PVsyst to account for the exponential dependence of R_{sh} on irradiance and for thin-film-specific recombination losses, improving simulation accuracy across all commercially available module technologies.

2.1.3 Temperature and Irradiance Dependence

PV cell performance is strongly dependent on both irradiance (G) and cell temperature (Tc). The photocurrent scales approximately linearly with irradiance: $I_{ph}(G) = I_{ph,STC} \times (G/G_{STC})$. Cell temperature, however, has a dominant negative effect on open-circuit voltage (VOC), which decreases at a rate of approximately -2.3 mV/°C for crystalline silicon [19]. Consequently, high-temperature conditions such as those experienced by the Brno province in summer reduce both VOC and module efficiency, which directly reduces the performance ratio, as quantified in Chapter 4 of this study. The temperature coefficient of maximum power (gamma) for the JinkoSolar 435 Wp module used in this study is -0.35%/°C, consistent with industry-standard monocrystalline silicon modules [20].

2.1.4 Real-World Performance Sensitivity

These physical dependencies - the linear relationship between photocurrent and irradiance, and the negative thermal sensitivity of open-circuit voltage - have direct consequences for real-world system performance that motivate the analytical framework of this thesis. A PV module operating outdoors rarely encounters the standard test conditions (G = 1000 W/m^2, Tc = 25°C) under which its rated power is specified. Irradiance varies continuously with solar angle, cloud cover, and atmospheric turbidity; cell temperature commonly exceeds STC by 20–30°C under full summer irradiance, with every degree above 25°C reducing maximum power output by approximately 0.35% for monocrystalline silicon modules [21]. Shading from adjacent structures or accumulated soiling reduces effective irradiance non-uniformly across the array, triggering disproportionate power losses through reverse-biased cell behavior that exceed the shaded fraction alone [22]. Module-to-module manufacturing tolerances create current mismatch within strings, further reducing array output below the sum of individual module ratings [23]. Each of these deviations from STC translates into a measurable reduction in output relative to the nameplate rating. The system performance indicators defined in Section 2.3 - and in particular the Performance Ratio - are specifically designed to quantify the aggregate effect of these real-world derating factors, and the loss decomposition framework of Chapter 4 isolates their individual contributions for each of the 13 Czech provinces.

2.2 Solar Radiation on Tilted Surfaces

2.2.1 Global Horizontal Irradiance Components

Total solar radiation incident on a horizontal surface global horizontal irradiance (GHI) is the sum of the direct normal irradiance (DNI) projected onto the horizontal plane and the diffuse horizontal irradiance (DHI) [19]:

(Eq. 2.2)

where is the solar zenith angle. For PV system design, the quantity of primary interest is the plane-of-array irradiance (POA or GPOA), which is the total irradiance incident on the tilted module surface and includes direct, diffuse, and ground-reflected (albedo) components [19], [20].

2.2.2 Optimal Tilt Angle Theory

The plane-of-array irradiance received by a fixed-tilt surface depends on the tilt angle (β), the azimuth angle (γ), the geographic latitude (φ), and the solar declination and hour angle. The annual-optimum tilt angle for a south-facing fixed surface in the Northern Hemisphere is generally close to the site latitude, with typical deviations of +/- 5 to 10 degrees depending on the diffuse fraction of the local climate [19]. For the Czech Republic (latitude 49-51 degrees N), the theoretically expected optimum is therefore approximately 44-46 degrees. The PVsyst optimization in this study yielded values of 38-42 degrees, which are systematically lower. This can be attributed to the relatively high diffuse radiation fraction in the Czech climate diffuse radiation is isotropic and does not benefit from steep tilts to the same degree as direct radiation and to the lower solar elevation angles in summer, which favor flatter tilts [20]. This is a non-trivial finding that distinguishes the Czech Republic from Mediterranean climates commonly studied in the literature.

2.2.3 Transposition Models

The conversion of GHI to POA irradiance requires a transposition model for the diffuse component. PVsyst implements the Perez anisotropic sky model, which accounts for circumsolar brightening and horizon brightening effects and outperforms isotropic models (such as Liu-Jordan) in accuracy for tilted surfaces, particularly under partly cloudy conditions prevalent in Central Europe [10], [20]. The Transposition Factor (FT = GPOA/GHI) quantifies the gain from panel tilt relative to horizontal collection. In this study, FT values range from 1.17 to 1.23 annually across Czech provinces, confirming that tilting from horizontal provides a 17-23% gain in intercepted radiation a key design justification for the 39-degree reference tilt adopted.

2.3 PV System Performance Indicators

2.3.1 Reference Yield (Y_r)

The reference yield (Y_r, kWh/kWp/day) is defined as the ratio of the total in-plane irradiation (HPOA, kWh/m^2) to the reference irradiance at standard test conditions (GSTC = 1 kW/m^2) [12]:

$$Y_r = HPOA / GSTC$$

(Eq. 2.3)

It represents the number of peak sun hours at the site and is independent of system losses, serving as the solar resource baseline for performance comparison.

2.3.2 Array Yield (Y_a)

The array yield (Y_a, kWh/kWp/day) is defined as the DC energy output of the array (E_{array}, kWh) normalized to the rated power of the system (P_0, kWp) [12]:

$$Y_a = E_{array} / P_0$$

(Eq. 2.4)

2.3.3 Final Yield (Y_f)

The final yield (Y_f, kWh/kWp/day) is the AC energy delivered to the grid (E_{grid}, kWh) normalized to rated power [12]:

$$Y_f = E_{grid} / P_0$$

(Eq. 2.5)

Y_f is the primary indicator of system productivity from the perspective of a building owner or grid operator.

2.3.4 Performance Ratio (PR)

The performance ratio is defined as the ratio of final yield to reference yield [12]:

$$PR = Y_f / Y_r$$

(Eq. 2.6)

PR is dimensionless and bounded between 0 and 1 (or expressed as a percentage). It captures the aggregate effect of all system losses thermal, wiring, mismatch, inverter, soiling relative to the available solar resource. A system operating without any losses would have PR = 1. In practice, well-designed grid-connected systems in temperate climates typically achieve PR values of 0.75-0.90 [12], [20]. The narrow range of 89.1%-89.7% observed across Czech provinces in this study indicates a well-configured and uniform system design, with provincial differences driven primarily by thermal losses.

2.3.5 Capture Loss (L_c) and System Loss (L_s)

Capture loss ($L_c = Y_r - Y_a$) quantifies array-level losses including thermal derating, wiring resistance, module quality, IAM losses, and mismatch. System loss ($L_s = Y_a - Y_f$) captures inverter conversion losses. Together, $L_c + L_s = Y_r - Y_f$ = total normalized losses, providing a diagnostic decomposition of system underperformance [12].

2.4 Grid-Connected PV System Architecture

A grid-connected PV system for residential buildings consists of four primary subsystems: (i) the PV array, (ii) the DC wiring and protection circuit, (iii) the grid-tied inverter, and (iv) the AC connection to the building distribution panel and utility grid [20]. Unlike stand-alone systems, grid-connected systems do not incorporate battery storage in the baseline configuration; surplus energy is exported to the grid, and deficits are covered by grid import.

The inverter performs two critical functions: DC-to-AC power conversion at near-unity power factor, and maximum power point tracking (MPPT). MPPT algorithms continuously adjust the operating voltage of the PV array to extract maximum power under varying irradiance and temperature conditions. The Huawei SUN2000-12KTL-M2 inverter used in this study employs dual-MPPT tracking across two independent string inputs, allowing the two 14-module strings to be optimized independently, which reduces mismatch losses relative to a single-MPPT configuration [10].

The string sizing criterion requires that the maximum open-circuit voltage of the string ($N \times V_C$, STC × correction factor for minimum temperature) does not exceed the inverter's maximum input voltage (950 V in this case), and that the minimum operating voltage at maximum power point under high-temperature conditions remains above the lower bound of the inverter's Full Power MPPT Voltage Range (360 V for this model), to avoid power clipping at full output. For the 14-module string with JinkoSolar 435 Wp modules (V_C = 39.16 V at STC), the string V_C at STC is 14 × 39.16 = 548.2 V, which satisfies the inverter constraint with adequate headroom [20].

2.5 nZEB Standards and the EPBD Framework

The concept of the nearly zero-energy building (nZEB) was introduced into EU law through Directive 2010/31/EU (EPBD), which required all new buildings to meet nZEB standards by 31 December 2024 [3]. The recast EPBD (Directive 2024/1275/EU) strengthens this framework by requiring all new buildings to be zero-emission buildings (ZEB) by 2030, defined as buildings with very high energy performance where the remaining energy demand is fully covered by on-site renewable sources or the energy grid [3]. Marszal et al. [24] identify on-site electricity generation primarily through rooftop PV as the dominant supply-side strategy for achieving net-zero energy balance in residential buildings.

In the Czech national context, the nZEB standard is implemented through Decree No. 264/2020 Coll., which defines minimum primary energy requirements for new constructions. A typical Czech single-family house has an annual heating demand of 50-80 kWh/m^2 and a total primary energy consumption of approximately 90-130 kWh/m^2/year. Assuming a representative Czech single-family house of 100 m^2 with a primary energy consumption of 90–130 kWh/m^2/year (total 9,000–13,000 kWh/year, per Decree No. 264/2020 Coll.), the 12 kWp system modelled in this thesis generates 13,169–14,533 kWh/year. Under a full self-consumption scenario - a theoretical upper bound - this corresponds to a primary energy offset of 40–58% of annual demand. Residential PV systems without battery storage generally achieve self-consumption rates of approximately 25–35%, depending on household load patterns and system sizing; similar values are reported for Czech household installations [25], yielding a net demand reduction of 10–20%. The spatial variation in system yields across Czech provinces documented here directly informs the feasibility of nZEB compliance through PV for different building locations, which is a finding of direct regulatory relevance.

2.6 Monte Carlo Simulation and Sensitivity Analysis

Monte Carlo (MC) simulation is a probabilistic computational method in which model inputs are represented as random variables sampled from prescribed probability distributions, and the model is evaluated across a large ensemble of realizations N to characterize the statistical distribution of outputs [13]. For a PV performance model g(theta), where $\theta = (G_{POA}, T_{amb}, \eta_{mod}, \eta_{inv}, f_{loss})$ is the vector of uncertain input parameters, the ensemble output Y(i) = g(theta(i)) is computed for each realization i = 1,...,N. The sample meaning and variance of Y are [13]:

(Eq. 2.7)

These statistics quantify the predictive uncertainty in Y_f and PR arising from natural variability in irradiance, temperature, and system parameters. The exceedance probability $P(Y > y)$ estimated from the empirical quantiles of the MC ensemble commonly reported as P90 (the yield exceeded in 90% of realizations) is the standard metric used in bankable yield assessments for solar project financing [13], [26].

Sensitivity analysis complements MC uncertainty quantification by attributing output variance to individual inputs. The one-at-a-time (OAT) normalized sensitivity index used in this study is [13]:

(Eq. 2.8)

where is the perturbation ratio (10-25% in this study) and $X_{k,0}$ is the baseline value of input k. expresses the percentage change in output per percentage change in input an elasticity measure that allows direct comparison of factor importance regardless of unit. This OAT approach, while local (evaluated at a single point in the input space), is computationally efficient and provides actionable design guidance when combined with MC-based global uncertainty bounds [13].

2.7 Multivariate Statistical Methods

2.7.1 Principal Component Analysis (PCA)

PCA is a linear dimensionality reduction technique that transforms a set of correlated variables into a smaller set of uncorrelated principal components (PCs), each capturing a decreasing fraction of total variance [27]. For a data matrix X (n provinces x p performance variables), PCA solves the eigenvalue problem of the covariance matrix: $C = (1/(n-1)) \times X^T \times X$. The first PC captures the direction of maximum variance; subsequent PCs are orthogonal to all preceding ones. In this study, PCA applied to the matrix of performance indicators (Y_f, PR, E_{grid}, total losses, T_{amb}, GHI) reveals that two principal components explain 62.5% of total variance, confirming that the spatial performance differentiation across Czech provinces can be adequately described by two dominant drivers: solar resource intensity and thermal derating.

2.7.2 K-means and Hierarchical Clustering

K-means clustering partitions n observations into k clusters by minimizing the within-cluster sum of squared Euclidean distances [27]. The algorithm iterates between assigning each observation to the nearest centroid and recomputing centroids until convergence. Hierarchical agglomerative clustering builds a dendrogram by successively merging the two closest clusters (using Ward's linkage criterion, which minimizes total within-cluster variance at each merge step) and does not require pre-specification of k. Both methods are applied here to the standardized PV performance dataset to identify province groups with shared system behavior, which is a prerequisite for region-differentiated policy design.

Chapter 3: Methodology

3.1 Research Design

This study follows a simulation-based quantitative research design structured in four sequential phases: (i) meteorological data acquisition and geographic characterization; (ii) PV system design and deterministic simulation in PVsyst v7; (iii) probabilistic uncertainty and sensitivity analysis via Monte Carlo methods in MATLAB 2019b; and (iv) spatial and multivariate statistical analysis. The four phases are independent in execution but sequentially dependent in data flow the deterministic simulation outputs serve as baseline inputs to the Monte Carlo framework, whose results in turn feed the multivariate analysis. This structure is consistent with established best practice for multi-province PV performance assessment [12], [20].

3.2 Study Area and Province Selection

The Czech Republic (49.44°N, 15.32°E) was selected as the study area on the basis of three criteria: (i) its moderate continental climate with distinct seasonal solar irradiance variation, representative of a broad class of Central European building contexts; (ii) the availability of province-level geographic data across its administrative units (NUTS 3 regions); and (iii) the relevance of its rapidly expanding residential PV market, as documented in Chapter 1. The Czech Republic comprises 14 NUTS 3 regions; of these, 13 provincial capitals were included in this study. Středočeský kraj was excluded because it is the only region without a distinct provincial capital city - its administrative seat is Prague, which is itself a separate, self-governing NUTS 3 region and is already represented in this study. Simulating an arbitrary point within Středočeský kraj without a defined urban center would introduce an inconsistency in site selection criteria relative to the other 13 city-based simulations. The 13 provinces included therefore represent complete coverage of all distinct urban administrative centers in the Czech NUTS 3 system.

The geographic characteristics of the 13 provinces latitude, longitude, and altitude were obtained from the Meteonorm 8.1 database integrated within PVsyst v7, as summarized in Table 1 [28], [29]. Altitude ranges from 151 m (Usti nad Labem) to 524 m (Jihlava), a variation sufficient to produce meaningful differences in ambient temperature, atmospheric pressure, and diffuse radiation fraction.

Table 1. Geographic characteristics of the 13 Czech provinces used in the study

Province	Latitude (N)	Longitude (E)	Altitude (m)	Climate Zone
Prague	50.10	14.26	364	Cfb
Zlin	49.22	17.67	228	Cfb
Ceske Budejovice	48.97	14.47	389	Dfb
Plzen	49.74	13.37	324	Cfb
Karlovy Vary	50.23	12.87	364	Cfb
Usti nad Labem	50.66	14.03	151	Cfb

Liberec	50.76	15.05	366	Cfb
Hradec Kralove	50.18	15.83	235	Cfb
Pardubice	50.04	15.77	215	Cfb
Jihlava	49.36	15.59	524	Dfb
Brno	49.19	16.60	229	Cfb
Olomouc	49.59	17.25	216	Cfb
Ostrava	49.78	18.27	242	Cfb

3.3 Meteorological Data

Hourly meteorological time series for each province were generated using Meteonorm 8.1, a globally validated stochastic weather generator developed by Meteotest AG (Bern, Switzerland). Meteonorm constructs synthetic typical meteorological year (TMY) files through interpolation of long-term ground station measurements and satellite data, using a Markov chain model for daily global horizontal irradiance and an autoregressive model for sub-daily disaggregation. For Version 8.1, the radiation reference period is 1996-2015 and the temperature reference period is 2000-2019, incorporating the most recent available satellite irradiance climatology [28].

The key meteorological parameters retrieved for each province are: global horizontal irradiance (GHI, kWh/m^2), diffuse horizontal irradiance (DHI, kWh/m^2), ambient temperature (Tamb, degrees), wind speed at 10 m height (m/s), and albedo coefficient. These parameters constitute the primary inputs to the PVsyst simulation engine. The spatial uncertainty of Meteonorm interpolation for European locations is reported as 2-10% for annual GHI [28], which is explicitly propagated through the Monte Carlo framework described in Section 3.6.

3.4 PV System Configuration

A standardised 12 kWp grid-connected rooftop PV system was designed to be representative of a Czech single-family dwelling. The 12 kWp capacity was selected to match the available net rooftop area of 56 m^2 consistent with the median rooftop area for Czech single-family houses and to align with the average domestic installation size of approximately 11.4 kWp recorded nationally in 2025 [6]. The system configuration is held constant across all 13 provinces to enable unconfounded spatial comparison of performance metrics. For the purpose of nZEB coverage calculations reported in Sections 4.7 and 5.1, a reference Czech single-family house of 100 m^2 gross floor area and a primary energy intensity of 90–130 kWh/m^2/year is assumed, consistent with the national standard under Decree No. 264/2020 Coll. This assumption is held constant across all provinces to ensure that provincial differences in coverage percentage reflect only differences in E_{grid}, not differences in reference building demand.

3.4.1 PV Modules

The JinkoSolar Tiger Neo N-Type JKM435N-54HL4R-V module (435 Wp) was selected on the basis of three criteria: (i) it is commercially available in the Czech market; (ii) its N-type TOPCon cell technology yields lower temperature coefficients relative to standard p-type PERC modules, making it appropriate for the temperate Czech climate; and (iii) its complete electrical characterisation data is available in the PVsyst module database. Key electrical parameters at standard test conditions (STC: G = 1000 W/m^2, Tc = 25 degrees, AM1.5) are: Pmax = 435 Wp, V_{OC} = 39.16 V, ISC = 13.80 A, V_{mp} = 32.59 V, Imp = 13.35 A, module efficiency = 21.77%, temperature coefficient of Pmax: gamma = -0.35%/degrees [30].

3.4.2 Inverter

The Huawei SUN2000-12KTL-M2 three-phase string inverter (12 kW rated AC output) was selected for its dual-MPPT capability, enabling independent optimization of each string, and its wide input voltage range (160-950 V DC), which ensures stable MPPT operation across the full range of seasonal irradiance conditions in the Czech Republic. Maximum inverter efficiency is 98.5% at rated power [31]. The DC/AC ratio of 12.18 kWp / 12 kW = 1.015 is within the recommended range of 1.0-1.3 for Central European climates [20].

3.4.3 Array Configuration

The PV array consists of two parallel strings of 14 modules each (28 modules total, 12.18 kWp installed). Each string is connected to one independent MPPT input of the inverter. The string voltage at STC is 14 × V_C = 14 × 39.16 = 548.2 V, well within the inverter's maximum input voltage of 950 V. The minimum string voltage at maximum power point under high-temperature operating conditions (T_C = 75°C, G = 800 W/m^2) is estimated at approximately 14 × 32.59 × (1 - 0.0028 × 50) = 14 × 28.03 ≈ 392.4 V. Per the manufacturer's datasheet, this exceeds the lower bound of the inverter's Full Power MPPT Voltage Range (360 V) with a margin of approximately 32 V - narrower than the previously stated 260 V, but still sufficient to avoid clipping under the assumed conditions. These sizing constraints confirm electrical compatibility per IEC 62548 [32].

3.4.4 System Losses and Parameters

The loss parameters entered PVsyst were assigned based on manufacturer specifications and published default values for comparable systems [20], [33]. Module quality loss was set to -0.8% (positive gain, as N-type TOPCon modules typically outperform STC ratings in the field). Module mismatch loss was set to 2% of array output. Ohmic wiring losses were set to 1.5% (DC side), corresponding to a cable cross-section of 6 mm2 and a maximum string run length of approximately 20 m. Soiling loss was set to 2% annually, consistent with temperate European conditions where rainfall provides regular panel cleaning. Inverter efficiency was modelled using the manufacturer's measured efficiency curve.

3.5 PVsyst Simulation Workflow

PVsyst v7 was used as the simulation platform. The simulation followed a four-step workflow consistent with the PVsyst v7 tutorial for grid-connected systems [34]:

Step 1: Site definition: Province coordinates and altitude were entered, and the Meteonorm 8.1 TMY file was loaded as the meteorological input. Horizon shading was set to zero (no near-shading) for all provinces, in accordance with the scope limitation stated in Section 1.5.

Step 2: Orientation optimization: The optimal tilt angle (β) and azimuth (set to 0 degrees = true south) were determined using PVsyst's built-in orientation optimization tool, which maximizes annual GHI on the collector plane by evaluating the Transposition Factor across all tilt angles from 0 to 90 degrees. The optimal tilt was determined independently for each province and verified against the theoretical expectation from Duffie and Beckman [19].

Step 3: System definition: The module and inverter were selected from the PVsyst database, the array configuration was entered (2 strings x 14 modules, dual MPPT), and all loss parameters were assigned as specified in Section 3.4.4.

Step 4: Simulation and output: The annual energy simulation was executed, producing monthly and annual values for all performance indicators defined in IEC 61724-1:2017: Y_f, PR, Y_a, Y_r, L_c, L_s, E_{grid}, and the full loss decomposition (thermal, wiring, mismatch, IAM, module quality, inverter losses). These outputs were exported for use in subsequent analysis phases.

3.6 Monte Carlo Uncertainty and Sensitivity Analysis

3.6.1 Input Variable Distributions

Six input parameters were treated as uncertain random variables, each assigned a probability distribution based on the best available evidence in the literature [13], [26]:

(i) Plane-of-array irradiance (GPOA): Normal distribution with mean equal to the Meteonorm TMY value and coefficient of variation (CV) = 5%, reflecting the combined uncertainty of the Meteonorm interpolation model and inter-annual irradiance variability for Central European locations.

(ii) Ambient temperature (T_{amb}): Normal distribution, CV = 3%, based on Meteonorm reported temperature uncertainty.

(iii) Module efficiency / temperature coefficient: Normal distribution, CV = 2%, based on manufacturer tolerance of +/-3% for Pmax.

(iv) Inverter efficiency: Uniform distribution within +/-1% of rated efficiency curve values, consistent with IEC 61683 inverter testing tolerances.

(v) Soiling loss factor: Uniform distribution [1%, 4%], reflecting seasonal variation in soiling accumulation and cleaning frequency under Central European conditions.

(vi) Ohmic wiring loss: Normal distribution, CV = 10%, reflecting uncertainty in actual cable lengths and contact resistances.

3.6.2 Simulation Procedure

N = 1000 Monte Carlo realizations were generated for each province using Latin Hypercube Sampling (LHS) implemented in MATLAB 2019b. LHS ensures more uniform coverage of the input space compared to simple random sampling at equivalent N, reducing the required sample size for stable quantile estimation. For each realization i, the perturbed input vector θ (i) was used to scale the deterministic PVsyst baseline outputs proportionally, consistent with the one-diode model framework described in Chapter 2. The ensemble outputs Y_f(i) and PR(i) were used to compute the sample statistics defined in Equation 2.7, as well as the P50 and P90 yield estimates relevant to bankable yield assessment.

3.6.3 Sensitivity Index Computation

The OAT normalized sensitivity index (Equation 2.8) was computed for each of the six input variables and each province, using a perturbation ratio Delta = 10%. The resulting sensitivity indices were ranked to produce a tornado diagram identifying the dominant performance drivers at the provincial and national scale. This ranking directly informs the policy discussion in Chapter 4, identifying which provinces require the most robust adaptive design strategies. To rank provinces by overall exposure to input uncertainty, an aggregate sensitivity score (ASS) is defined as the sum of the six per-variable OAT sensitivity indices for each province:

(Eq. 3.1)

where is the OAT sensitivity index (Eq. 2.8) of input variable k for province p. Unlike the individual values - which are bounded approximately [0, 1] and used to identify the dominant driver within a province - the ASS aggregates across all six input variables to rank provinces by their total exposure to input variability. This aggregate score is used to construct the tornado diagram in Figure 4.7C and the radar profile in Figure 4.7D.

3.7 Spatial and Multivariate Statistical Analysis

3.7.1 Spatial Mapping

The annual performance metrics (Y_f, PR, E_{grid}, total losses) were georeferenced to province centroid coordinates and interpolated across the Czech Republic using inverse distance weighting (IDW) to produce continuous spatial distribution maps. IDW was selected over kriging due to the limited number of spatial observation points (n = 13), for which variogram estimation required by kriging is unreliable [27]. The spatial maps were generated in MATLAB 2019b using the grid data function with the IDW kernel.

3.7.2 Principal Component Analysis

PCA was applied to the standardized (zero-mean, unit-variance) matrix of six performance and climate variables: Y_f, PR, E_{grid}, total system losses, mean annual T_{amb}, and annual GHI. Standardization is mandatory before PCA when variables have different units and scales, to prevent variables with large absolute magnitudes from dominating the principal components [11]. The eigen decomposition of the covariance matrix was computed using MATLAB's pca() function, and the results are reported as a scree plot (explained variance per PC) and a biplot showing province loadings in the PC1-PC2 plane.

3.7.3 Clustering

K-means clustering (k = 3, determined by the elbow method applied to within-cluster sum of squares versus k) and hierarchical agglomerative clustering (Ward linkage) were applied to the standardized performance matrix. For K-means, 100 random initializations were used and the solution with minimum total within-cluster variance was retained. The hierarchical dendrogram provides a complementary visualization of province groupings that does not require pre-specification of k, enabling validation of the K-means partition.

3.8 Reproducibility and Data Availability

All simulations were conducted in PVsyst v7.4.3 and MATLAB R2019b. The PVsyst project files (.vsf), the MATLAB Monte Carlo scripts, and the province-level TMY meteorological files generated from Meteonorm 8.1 are available from the author upon request. The module datasheet and the PVsyst v7 tutorial are publicly accessible and are cited with full bibliographic details in the reference list. Simulation results are reported to three significant figures throughout, consistent with the precision of the meteorological input data.

Chapter 4: Results and Discussion

Before presenting the provincial results, the reliability of the PVsyst simulation platform is established. Ahmad et al. [14] validated PVsyst outputs against field-measured data for fixed-tilt and azimuth-tracking systems over five clear-sky days, reporting mean deviations of 2.14% and 2.74% respectively. These figures confirm that PVsyst operates within the accepted 5% accuracy threshold for bankable yield assessment. All deterministic results in this chapter carry an implicit simulation uncertainty of approximately +/-2-3%; probabilistic bounds are established separately in Section 4.5.

4.1 Tilt Angle Optimization and Solar Resource on the Collector Plane

4.1.1 Annual Transposition Factor and Optimal Tilt

Figure 4.1 presents the annual tilt optimization analysis for all 13 provinces, showing (A) the Transposition Factor (FT), (B) energy losses relative to the optimal tilt, and (C) total annual irradiation on the collector plane.

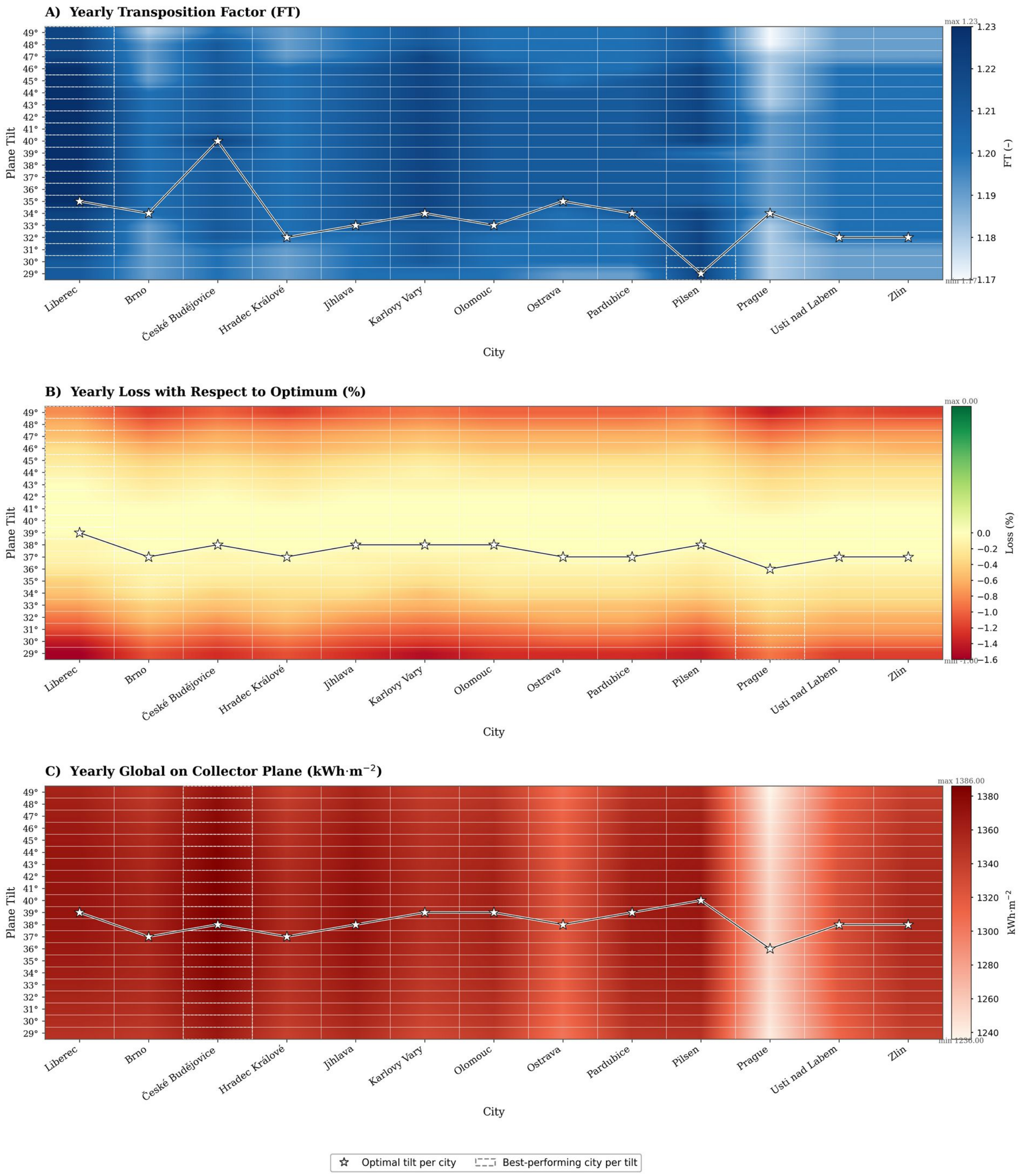

Figure Results and Discussion.3. Annual tilt optimization: (A) Transposition Factor (FT = GPOA/GHI) across tilt angles 29-49 degrees, (B) energy losses relative to optimum (%), and (C) total annual irradiation on the collector plane (kWh/m^2), for all 13 Czech provinces.

The annual FT ranges from 1.17 to 1.23 across all provinces, confirming that a correctly tilted surface intercepts 17-23% more solar radiation than a horizontal surface - consistent with the theoretical expectation for latitudes 49-51 degrees N [19]. Liberec, Pardubice, and Hradec Kralove record the highest FT values. The optimal annual tilt angle lies between 38 degrees and 42 degrees across all provinces - systematically 8–12 degrees below the geographic latitude of 49–51 degrees N, with Prague showing the largest deviation (~12°) due to its comparatively low optimal tilt of 38° relative to its 50.1°N latitude, which is the standard rule-of-thumb for fixed-tilt systems [19]. The deviation arises from two effects: (i) the high diffuse radiation fraction in Czech C_{fb}/D_{fb} climates, which responds less to tilt than direct beam radiation; and (ii) the summer-dominant energy balance, which favors flatter tilts. Applying the latitude-matching rule in Czech residential construction would overestimate the optimal tilt by up to 12 degrees, resulting in energy losses quantifiable from Figure 4.1B.

Figure 4.1B shows that losses relative to the annual optimum remain below 1.6% across the full tilt range of 29–49 degrees, with the largest penalties occurring at low tilt angles for Prague and Plzeň, confirming that annual energy yield is only weakly sensitive to moderate deviations from the optimal tilt- a practically important result, as it implies that rooftop pitch constraints of +/-5 degrees from the optimum impose minimal energy penalties. The highest annual collector plane irradiation (Figure 4.1C, peak 1,386 kWh/m^2) is recorded in Ceske Budejovice, Jihlava, and Plzen, driven by clearer skies and higher direct beam fractions in the southern and western provinces. Prague consistently reports the lowest values, attributed to its urban microclimate - higher aerosol loading and more frequent fog - rather than to any latitude effect [28].

4.1.2 Seasonal Tilt Sensitivity

Figure 4.2 presents the seasonal tilt analysis, separately for summer and winter, revealing a pronounced asymmetry critical for fixed-tilt system design.

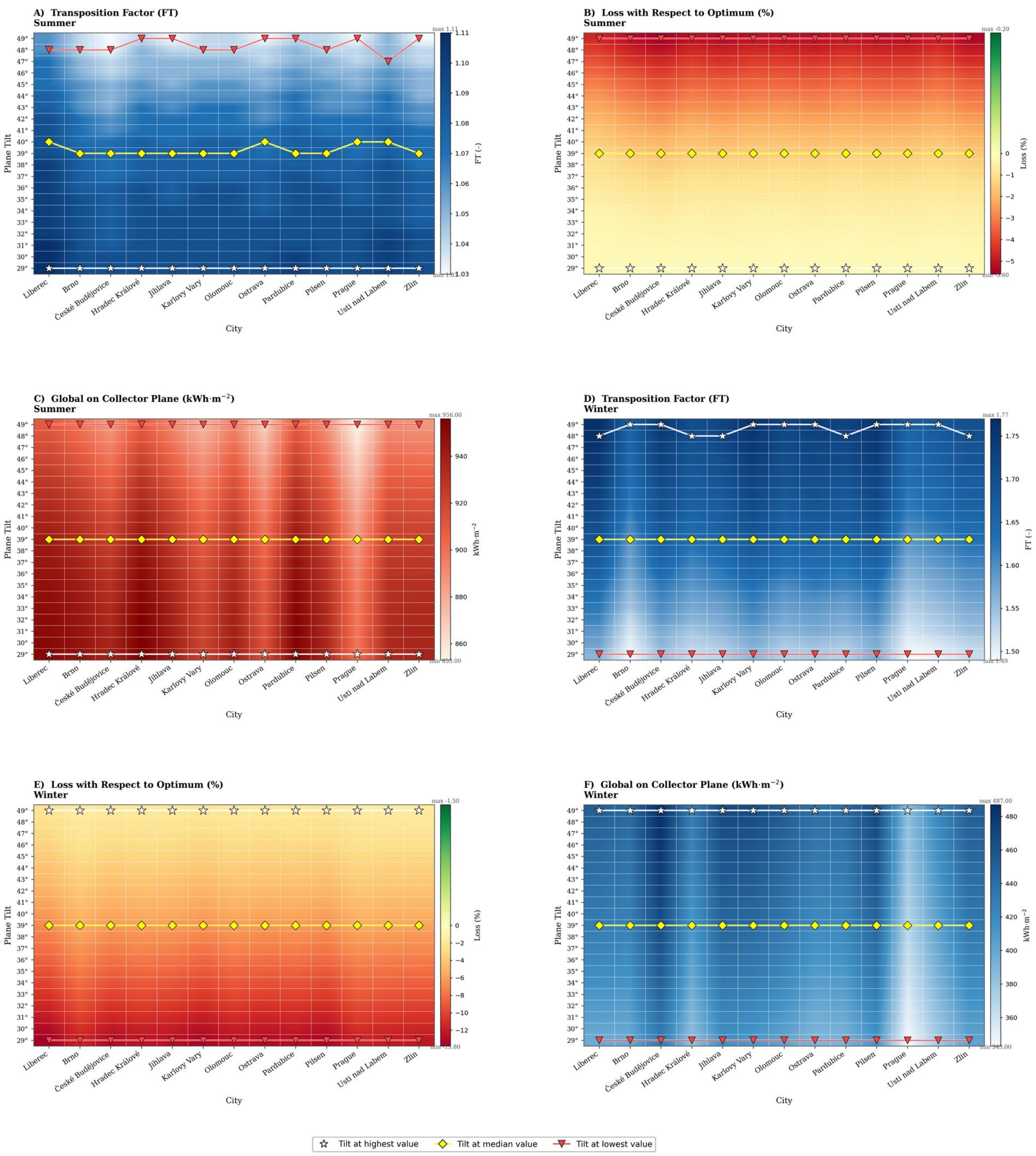

Figure Results and Discussion.4. Seasonal tilt optimization: Summer (A) FT, (B) losses relative to optimum, (C) collector plane irradiation; Winter (D) FT, (E) losses relative to optimum, (F) collector plane irradiation, for all 13 provinces.

During summer (Figure 4.2A-C), the FT-maximizing tilt is 29 degrees for all 13 provinces - the lower boundary of the tested tilt range (29–49°) - and FT ranges from 1.03 to 1.11, reflecting high solar elevation angles. Because the optimum sits at the edge of the tested range rather than an interior maximum, the true summer-optimal tilt may lie below 29 degrees; this is noted as a limitation of the tilt sweep resolution rather than a definitive optimum. A fixed tilt of 49 degrees in summer incurs losses up to 3% relative to the seasonal optimum (Figure 4.2B), a penalty that accumulates significantly given that summer months contribute approximately 65-70% of annual energy production [19]. Liberec achieves the highest summer FT, suggesting lower aerosol loading or higher direct beam fraction. Summer collector plane irradiance (Figure 4.2C) ranges from 853 to 956 kWh/m^2, with Hradec Kralove and Pardubice leading and Prague recording the lowest values.

In winter (Figure 4.2D-F), the relationship is reversed: FT rises to 1.49-1.77, nearly double the summer value. The optimal winter tilt is 45-49 degrees, and a sub-optimal tilt of 29 degrees incurs up to 13% energy loss (Figure 4.2E). Ceske Budejovice, Jihlava, and Plzen lead in winter collector plane irradiation (343-487 kWh/m^2, Figure 4.2F), while Prague records the lowest values for the third consecutive sub-analysis. This seasonal asymmetry demonstrates the fundamental design tension in fixed-tilt residential systems: the 38-42 degree annual optimum is a weighted compromise favoring summer yield, appropriate for the Czech energy balance but leaving winter performance sub-optimal [19].

4.2 Weather Variables and Incident Solar Energy

Figure 4.3 presents the monthly profiles of key weather and irradiance variables for the full annual period across all provinces.

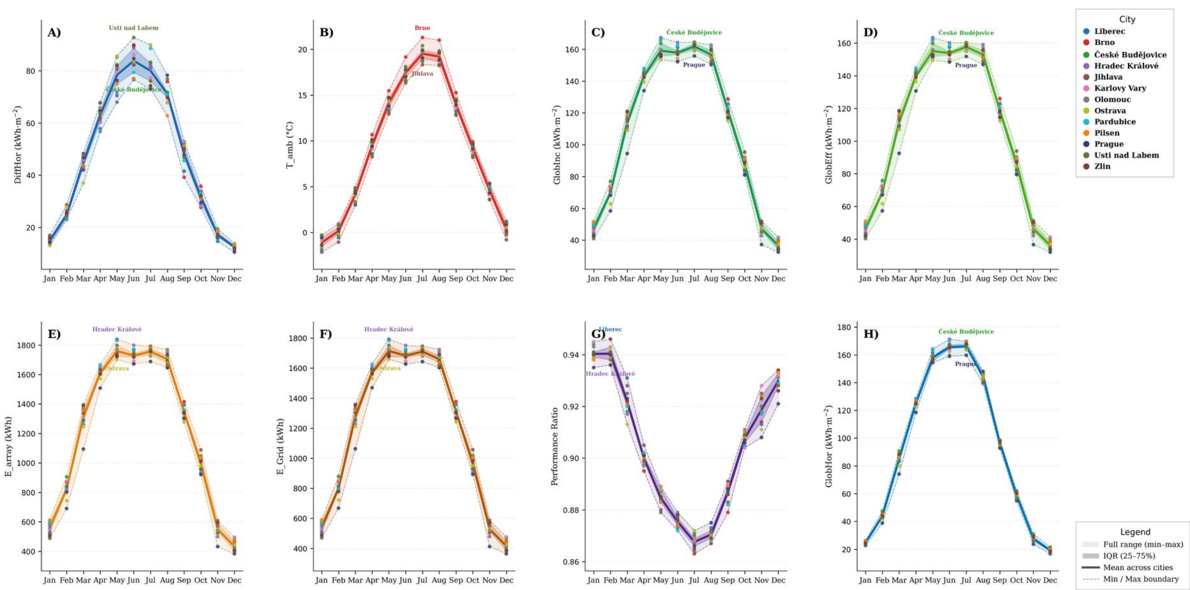

Figure Results and Discussion.5. Monthly weather and irradiance profiles: (A) diffuse horizontal irradiation DifHor (kWh/m^2), (B) ambient temperature T_{amb} (°C), (C) incident global irradiation on collector plane GlobInc (kWh/m^2), (D) effective global irradiation GlobEff (kWh/m^2), (E) DC array energy E_{array} (kWh), (F) energy injected to grid E_{Grid} (kWh), (G) performance ratio PR (%), (H) global horizontal irradiation GlobHor (kWh/m^2), for all 13 Czech provinces.

4.2.1 Diffuse Radiation and Sky Conditions

Figure 4.3A shows diffuse horizontal irradiance (DifHor) peaking in summer and declining in winter due to fog and atmospheric conditions. Inter-provincial variation is limited, but Usti nad Labem (92.77 kWh/m^2) and Ostrava (89.98 kWh/m^2) exhibit the highest diffuse fractions, consistent with elevated aerosol loading and cloud frequency in the northern and northeastern provinces [28], [35]. Under predominantly overcast conditions, the diffuse fraction increases while beam irradiance drops; PV modules continue to generate from diffuse radiation but at reduced efficiency [36].

4.2.2 Ambient Temperature and Thermal Derating

Figure 4.3B shows ambient temperature peaking in July across all provinces. Brno records the highest monthly peak at 21.28 °C in July, while Jihlava - at 524 m altitude - remains the coolest at 18.32 °C. The 2.96 °C difference, combined with the module temperature coefficient of -0.35%/°C [30], implies a power output difference of approximately 1.0% between the two provinces at peak summer conditions. Using the NOCT formula:

Assuming a nominal operating cell temperature (NOCT) of 43 °C, at G = 1000 W/m^2, cell temperature reaches approximately 50.1°C in Brno versus 47.1°C in Jihlava. The resulting power losses relative to STC are 8.8% and 7.7% respectively, directly explaining why Brno shares the lowest annual PR (89.1%) despite its higher irradiance [12]. Prague's low PR stems from a different mechanism - its comparatively poor tilt-latitude match and atmospheric effects, rather than thermal derating.

4.2.3 Collector Plane and Effective Irradiance

Figure 4.3C (GlobInc) and Figure 4.3D (GlobEff) show near-identical seasonal profiles, with minor differences representing IAM and soiling losses. Peak GlobInc values occur in May–June, with České Budějovice recording the highest incident irradiation and Prague the lowest across the annual cycle. The close agreement between GlobInc and GlobEff across all provinces confirms that soiling and angle-of-incidence losses are uniform and low under Czech temperate conditions [12], [34].

4.2.4 Array Energy, Grid Energy, and Performance Ratio

Figure 4.3E shows DC array energy (E_{array}) peaking in June at 1,840 kWh for Hradec Kralove and declining to lower values for Ostrava (1,726 kWh in May), consistent with Ostrava's comparatively lower irradiance and more frequently overcast conditions rather than thermal derating [37]. Figure 4.3F shows AC grid energy (E_{Grid}) following E_{array} closely, confirming high inverter performance and minimal conversion losses. Hradec Kralove, Liberec, and Pardubice consistently lead.

Figure 4.3G reveals the seasonal PR profile: PR drops in summer across all provinces due to elevated cell temperatures, reaching their minimum in July. Brno records the lowest mid-summer PR, consistent with its highest ambient temperatures. Provinces with cooler summer climates - Ostrava, Usti nad Labem, and Olomouc - maintain higher mid-summer PR values, confirming that thermal management rather than irradiance is the dominant within-season performance driver. Figure 4.3H (GlobHor) peaks in June-July, with Hradec Kralove and Pardubice showing a slight advantage in June and Plzen and Ceske Budejovice in July [38].

4.3 Wind, Diffuse on Collector Plane, and Albedo

Figure 4.4 presents three additional meteorological variables that modulate PV performance at the system level.

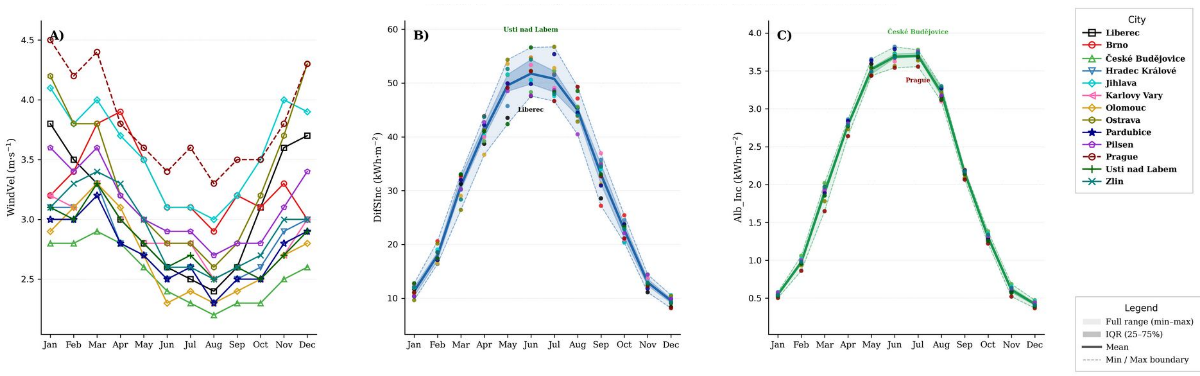

Figure Results and Discussion.6. Monthly profiles: (A) wind velocity WindVel (m/s), (B) incident diffuse irradiation on collector plane DifSInc (kWh/m^2), (C) albedo-reflected irradiation on module surface Alb_{Inc} (kWh/m^2), for all 13 Czech provinces.

Figure 4.4A shows wind velocity (WindVel) across provinces, with Prague and Jihlava exhibiting the highest values, peaking in January and December. Wind acts as a passive cooling mechanism: in PVsyst, higher wind speed reduces the thermal loss coefficient in the Faiman module temperature model, improving cell temperature and partially mitigating thermal derating. The cooling benefit for Jihlava - combining high altitude, low ambient temperature, and elevated wind - produces a compound performance advantage that contributes directly to its top PR ranking (89.7%) despite its southern location and modest irradiance compared to Ceske Budejovice [39].

Figure 4.4B shows incident diffuse irradiation on the collector plane (DifSInc), with Usti nad Labem recording the highest values and Liberec the lowest, consistent with more frequently overcast conditions in northern Bohemia. High DifSInc values maintain energy production when direct beam is limited, attenuating the performance gap between cloudy northern and clearer southern provinces. The Perez anisotropic transposition model in PVsyst captures this diffuse contribution accurately.

Figure 4.4C shows albedo-reflected irradiance (Alb_{Inc}), with České Budějovice recording the highest values and Prague the lowest. The fixed albedo coefficient of 0.20 (dry concrete/asphalt) is used throughout, which conservatively underestimates winter performance when seasonal snow cover can increase ground reflectance to 0.6-0.8. Andrews and Pearce demonstrated that albedo modification shifts optimal tilt angles and alters module spectral response, an effect amplified for bifacial modules [40]. The present monofacial system captures only the standard albedo contribution as computed by PVsyst.

4.4 System Loss Decomposition

Figure 4.5 presents the monthly loss decomposition across all provinces, isolating five distinct loss mechanisms.

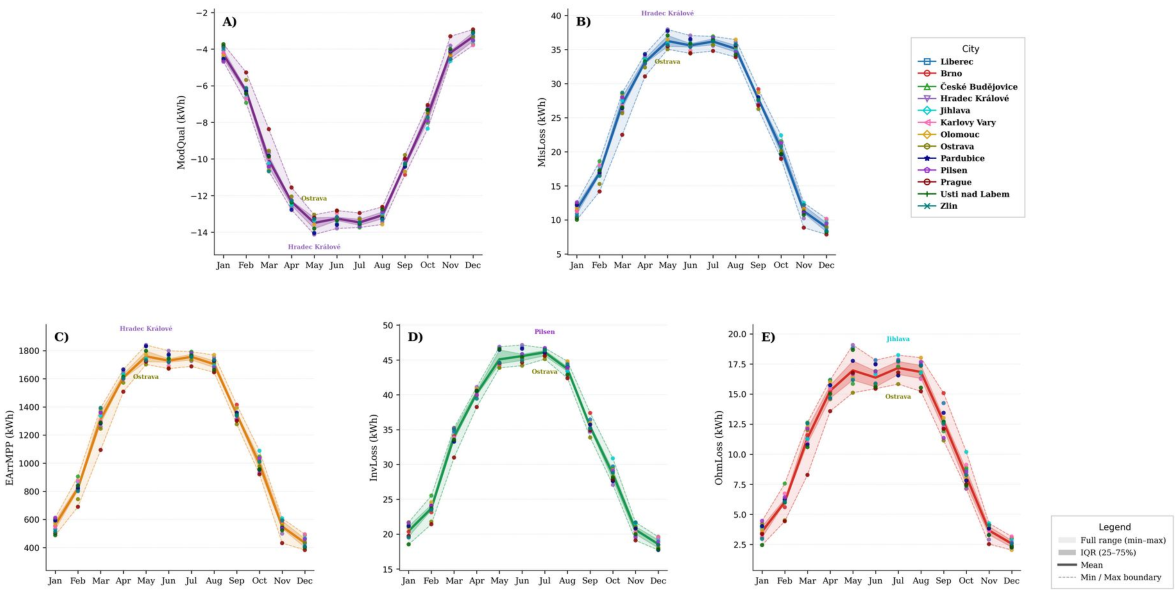

Figure Results and Discussion.7. Monthly system loss decomposition: (A) module quality loss ModQual (kWh), (B) module mismatch loss MisLoss (kWh), (C) array energy at MPP EArrMPP (kWh), (D) inverter conversion loss InvLoss (kWh), (E) ohmic wiring loss OhmLoss (kWh), for all 13 Czech provinces.

4.4.1 Module Quality Loss

Figure 4.5A shows module quality loss (ModQual) ranging from -14 kWh to -3 kWh — negative values indicating a net gain over STC-rated performance. This is characteristic of N-type TOPCon technology, which exhibits lower light-induced degradation (LID) and reduced recombination losses at the passivated tunnel oxide contacts relative to conventional p-type PERC modules [20]. The gain is uniform across provinces, confirming ModQual is a module-intrinsic property independent of site.

4.4.2 Mismatch Loss

Figure 4.5B shows mismatch loss (MisLoss) peaking in May-July at 37-38 kWh monthly and declining to 7.86 kWh in September. The seasonal pattern tracks irradiance variability: higher irradiance months create larger instantaneous power differences between modules operating under slightly different conditions, amplifying mismatch [23]. Hradec Kralove, Liberec, and Pardubice experience the highest absolute mismatch losses - consistent with their higher irradiance levels - while Ostrava shows below-average losses, reflecting its more uniform overcast irradiance conditions. The dual-MPPT configuration minimizes cross-string mismatch but cannot eliminate within-string module-level differences.

4.4.3 Array Energy at MPP

Figure 4.5C shows array energy at maximum power point (EArrMPP) peaking in May at 1,840 kWh for Liberec and Hradec Kralove, then declining significantly by September. Prague consistently underperforms the provincial means, reflecting its lower irradiance and higher thermal losses. This metric serves as the primary diagnostic of DC-side performance before inverter conversion losses are applied [12].

4.4.4 Inverter and Ohmic Losses

Figure 4.5D shows inverter conversion losses (InvLoss) peaking at 46-47 kWh monthly and declining to approximately 17 kWh in September, tracking the seasonal array output profile. Inter-provincial variation is minimal, as inverter efficiency is primarily load dependent. Ostrava and Olomouc show marginally lower inverter losses as a direct consequence of their lower array outputs. The Huawei SUN2000-12KTL-M2 achieves weighted annual efficiency of approximately 97.8%, consistent with manufacturer specifications. Figure 4.5E shows ohmic wiring losses (OhmLoss), proportional to the square of string current ($P_{loss} = I^2 \times R_{cable}$), peaking in summer. Hradec Kralove and Liberec record the highest monthly OhmLoss (18-19 kWh) as a direct consequence of their higher currents, while Prague's lower OhmLoss (16.8 kWh) is a mathematical consequence of lower array current, not a cable design advantage. Annual ohmic losses fall within 1.4-1.6% of array output across all provinces.

4.5 Normalized Performance Indicators

Figure 4.6 presents the normalized performance coefficient analysis for all provinces for full annual period, decomposing system performance into the standard IEC 61724-1:2017 metrics [12].

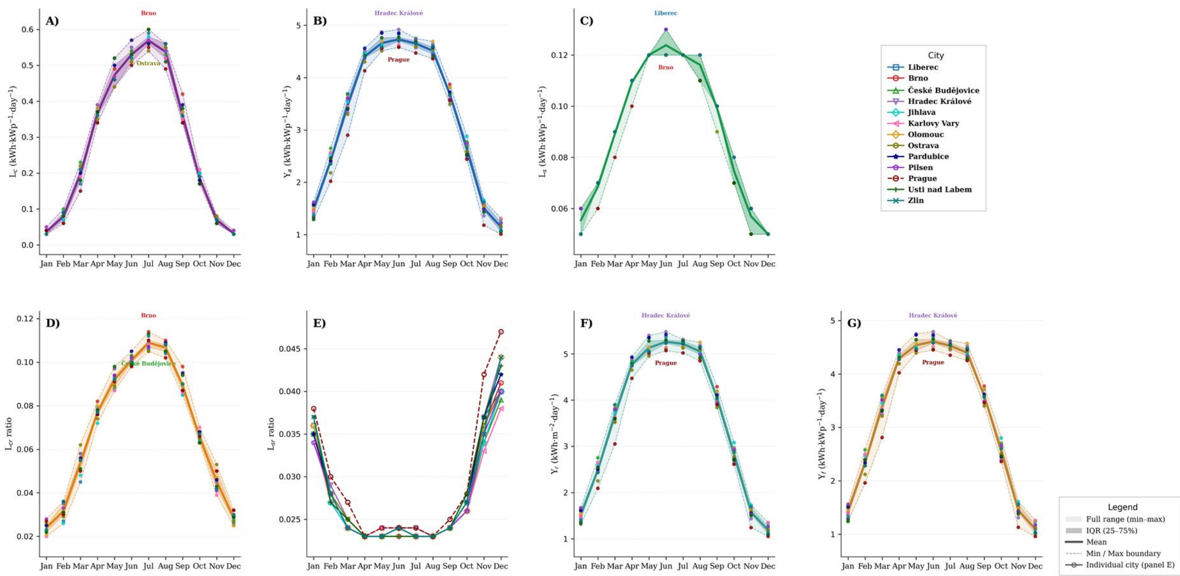

Figure Results and Discussion.8. Monthly normalized performance indicators: (A) capture loss L_c (kWh/kWp/day), (B) array yield Y_a (kWh/kWp/day), (C) system loss L_s (kWh/kWp/day), (D) capture loss ratio L_{cr}, (E) system loss ratio L_{sr}, (F) reference yield Y_r (kWh/m^2/day), (G) final yield Y_f (kWh/kWp/day), for all 13 Czech provinces.

Figure 4.6F (reference yield Y_r) peaks in May-June and tracks the GHI profile directly, with Hradec Kralove, Pardubice, and Liberec showing the highest values and Prague the lowest. This confirms that the inter-provincial irradiance gradient - not system design differences - drives the primary performance variation. Figure 4.6G (final yield Y_f) closely mirrors Y_r, with slight reductions due to real-world losses, confirming high system quality uniformly across all provinces. Liberec, Pardubice, and Hradec Kralove maintain the highest Y_f, while Prague records the lowest.

Figure 4.6A (capture loss L_c) peaks in July - the month of maximum thermal derating - and is highest for Brno, Zlin, and Usti nad Labem. This confirms that summer thermal losses constitute the dominant array-level inefficiency across Czech provinces. Figure 4.6B (Y_a) follows irradiance, peaking in June-July. Figure 4.6C (system loss L_s) remains near-constant across months and provinces, confirming that the inverter and wiring losses are systematically controlled and independent of geography.

Figure 4.6D (capture loss ratio $L_{cr} = L_c/Y_r$) peaks in June-July for Brno, Zlin, and Usti nad Labem, confirming temperature-related derating as the dominant fractional loss. Olomouc and Karlovy Vary perform better, showing lower L_{cr} - provinces with moderate temperatures and adequate wind cooling maintain proportionally lower array losses relative to the available resources. Figure 4.6E (system loss ratio L_{sr}) remains flat across all provinces and months, confirming that system-level losses are design-controlled and effectively uniform.

Table 2 summarizes the annual performance indicators for all 13 provinces, constituting the primary quantitative contribution of this thesis. All metrics are per IEC 61724-1:2017 [12].

Table 2. Annual PV system performance summary across 13 Czech provinces (12 kWp system).

Province	Y_f (kWh/kWp/day)	PR (%)	E_{grid} (kWh/yr)	Total Losses (kWh/yr)	Optimal Tilt (deg)
Prague	2.96	0.893	13169	1546.2	38
Ceske Budejovice	3.27	0.896	14533	1669.56	40
Plzen	3.21	0.894	14251	1663.32	41
Karlovy Vary	3.2	0.896	14213	1626.24	40
Usti nad Labem	3.16	0.893	14027	1655.4	39
Liberec	3.24	0.895	14423	1666.2	39
Hradec Kralove	3.19	0.892	14189	1688.28	40
Pardubice	3.22	0.892	14310	1706.16	40
Jihlava	3.26	0.897	14485	1633.92	40
Brno	3.21	0.891	14261	1721.16	41
Olomouc	3.23	0.895	14361	1666.44	40
Zlin	3.19	0.893	14199	1670.16	39
Ostrava	3.11	0.894	13846	1616.28	39

The PR range of 89.1%-89.7% is among the highest reported in the peer-reviewed literature for fixed-tilt grid-connected residential systems in temperate climates. Direct comparison across studies is limited by differences in system scale, module technology, and climate: Sahouane et al. [41] reported PR of 75–82% for a 28 kWp desert system in Algeria, where high irradiance and ambient temperatures above 35 °C produce severe thermal derating; Kumar et al. [39] reported 73–81% for a roof-integrated system in northern India under similar thermal stress; and Malvoni et al. [42] reported 78–83% for a 960 kWp utility-scale system in Mediterranean Italy. Despite these differences in system size and geography, the comparison is directionally valid: all three studies use silicon-based modules with temperature coefficients comparable to the JinkoSolar TOPCon module used here, and the common mechanism - thermal derating under high ambient temperatures - is absent in the Czech temperate climate, explaining the systematically higher Czech PR values. The narrow 0.6 percentage point spread across all 13

Czech provinces additionally confirms uniform system design quality independent of provincial location.

4.6 Monte Carlo Uncertainty Quantification and Sensitivity Analysis

Figure 4.7 presents the Monte Carlo sensitivity and correlation analysis across all 13 provinces.

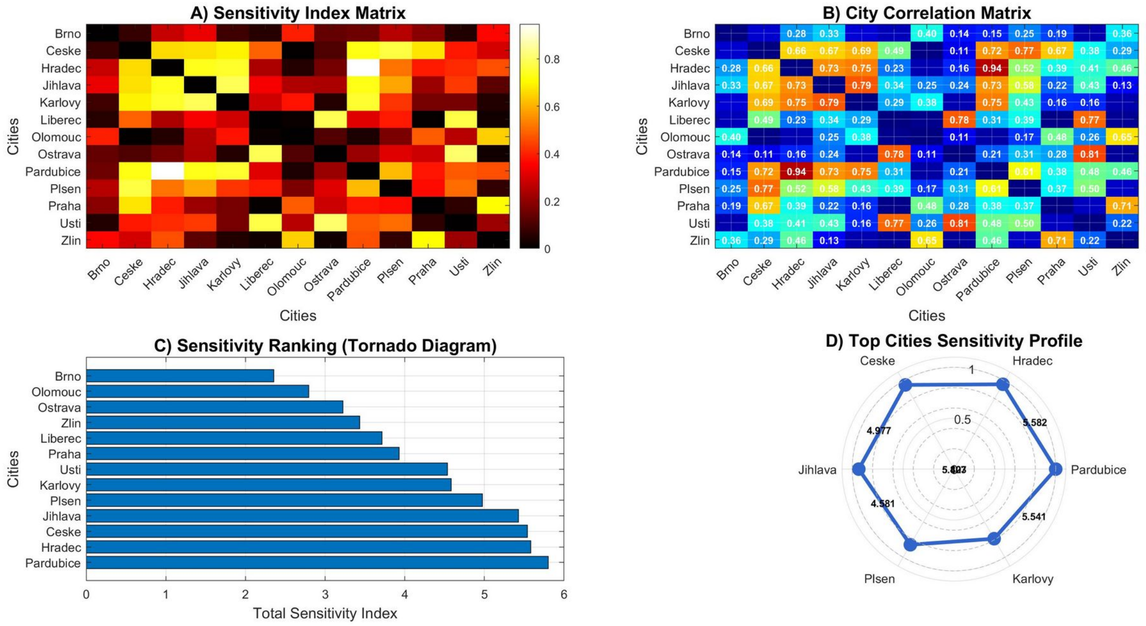

Figure Results and Discussion.9. Monte Carlo sensitivity analysis: (A) pairwise sensitivity index matrix (heatmap), (B) city correlation matrix, (C) sensitivity ranking tornado diagram - provinces ranked by contribution to yield variability, (D) radar profile of top-sensitivity provinces.

Figure 4.7A shows the pairwise sensitivity index matrix. Brighter colors indicate stronger performance interdependencies between province pairs, reflecting shared climatic drivers. Figure 4.7B shows the correlation matrix: Hradec Kralove and Pardubice display the strongest pairwise correlation in the matrix (r = 0.94), sharing similar irradiance and temperature regimes - as do Karlovy Vary and Jihlava (r = 0.79) and Ostrava and Usti nad Labem (r = 0.81). In contrast, Jihlava and Zlin show one of the weakest inter-correlations (r = 0.13), indicating more independent performance trajectories [26].

Figure 4.7C (tornado diagram) ranks provinces by their aggregate sensitivity score (ASS) - their relative contribution to national yield variability. Pardubice (ASS ≈ 5.80), Hradec Kralove (≈ 5.58), and Ceske Budejovice (≈ 5.50) emerge as the most sensitive provinces, while Brno (≈ 2.30) and Olomouc (≈ 2.75) show the lowest sensitivity. Figure 4.7D (radar profile) shows the top six provinces by ASS: Pardubice, Hradec Kralove, Karlovy Vary, Jihlava, Ceske Budejovice, and Plzen - a cluster of provinces exhibiting the highest combined exposure to input variability. Notably, Praha is not among these top-sensitivity provinces despite its comparatively low absolute yield (ASS ≈ 3.9, ranked 8th of 13) - indicating that Praha's underperformance stems from a structurally lower resource baseline rather than from disproportionate sensitivity to weather variability. This is consistent with Praha's separate Value-at-Risk profile: Praha still records the lowest VaR at the 5% quantile of any province (VaR5% = 3.051 kWh/kWp/day), reflecting the same lower absolute floor. Together, these results indicate Praha's primary planning concern is its structurally lower baseline resource availability, not output volatility - unlike Pardubice or Hradec Kralove, which combine solid average performance with high sensitivity to year-to-year weather variation.

The Monte Carlo ensemble (N = 1000 realizations per province) yields a national mean expected annual Y_f of 3.17 kWh/kWp/day with a coefficient of variation (CV) of 3.2%. At the portfolio level, the expected total output is 42.71 +/- 1.20 normalized units with a 95% confidence interval of [40.39, 45.09], confirming robust systemic reliability through geographic diversification [13], [26]. The aggregate portfolio CV (2.8%) is lower than the mean provincial CV (4.3-4.5%), demonstrating the risk-reduction benefit of geographic spread - a principle central to energy systems planning.

The OAT sensitivity analysis identifies plane-of-array irradiance (G_{POA}) as the dominant driver with normalized sensitivity indices of 0.85-0.95, confirming that meteorological uncertainty is the primary source of performance risk. Ambient temperature ranks second (indices 0.20-0.35, negative sign). Module efficiency uncertainty ranks third (0.15-0.25). Inverter efficiency, soiling, and ohmic losses each contribute indices below 0.10. For building designers, this hierarchy implies that improving meteorological data quality yields a greater reduction in performance uncertainty than any system component optimization [13], [26]. Within the present TMY-based framework, this limitation is partially addressed by treating GPOA as a stochastic variable with a 5% coefficient of variation in the Monte Carlo ensemble; however, this parameterization is itself derived from Meteonorm uncertainty estimates rather than from measured inter-annual records. For future installations, on-site irradiance measurement over at least one pre-installation year would provide an empirically grounded uncertainty bound superior to the TMY-derived estimate used here.

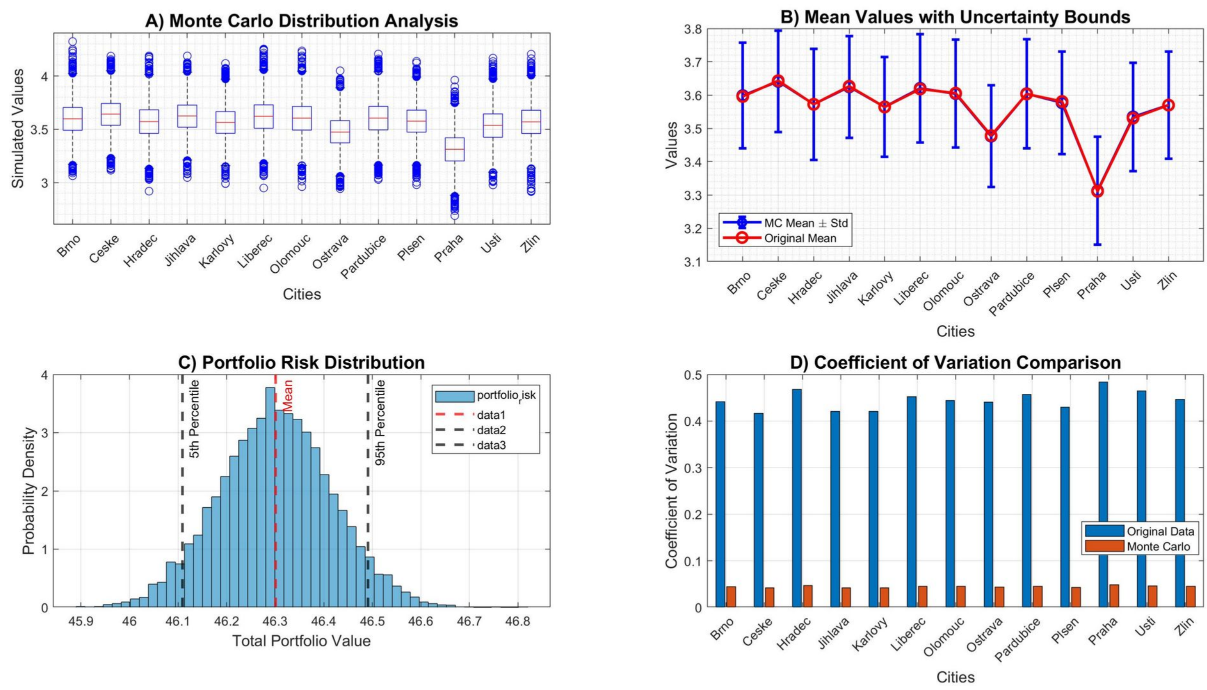

Figure Results and Discussion.10. Monte Carlo output distributions: (A) distribution of simulated annual Y_f outcomes per province, (B) mean values with 95% uncertainty bounds, (C) portfolio risk distribution for all provinces combined, (D) coefficient of variation comparison between original data and Monte Carlo simulations.

Figure 4.8A shows the full Monte Carlo output distributions per province. Usti nad Labem, Hradec Kralove, and Jihlava display the widest spreads - highest exposure to climatic uncertainty - while Brno, Plzen, and Prague demonstrate narrower, more predictable distributions. Figure 4.8B shows mean values with uncertainty bounds: Usti nad Labem and Ostrava exhibit larger margins, while Prague and Brno show smaller deviations. This differentiation is critical for policy: applying a uniform national incentive structure ignores the fundamentally different risk profiles of Czech provinces, potentially leading to under-preparedness in high-variability provinces [43].

Figure 4.8C presents the aggregate portfolio risk distribution, demonstrating systemic stability through the balancing effect of geographically diverse generation. Figure 4.8D compares the coefficient of variation computed from the original weather/yield data against the post-simulation Monte Carlo ensemble: the raw inter-annual CV ranges from ~0.42 to ~0.48 across provinces, with Hradec Kralove and Praha exhibiting the highest relative variability and Ceske Budejovice, Jihlava, and Karlovy Vary the lowest, while Olomouc and Zlin remain near the provincial average. The Monte Carlo ensemble CV is uniformly much lower (~0.04–0.05) across all provinces, reflecting the reduction in output variability once weather-driven yield is propagated through the full simulation chain rather than measured directly from raw historical records [44].

4.7 Spatial Distribution Analysis

Figure 4.9 presents the spatial distribution maps of four key performance metrics across the Czech Republic.

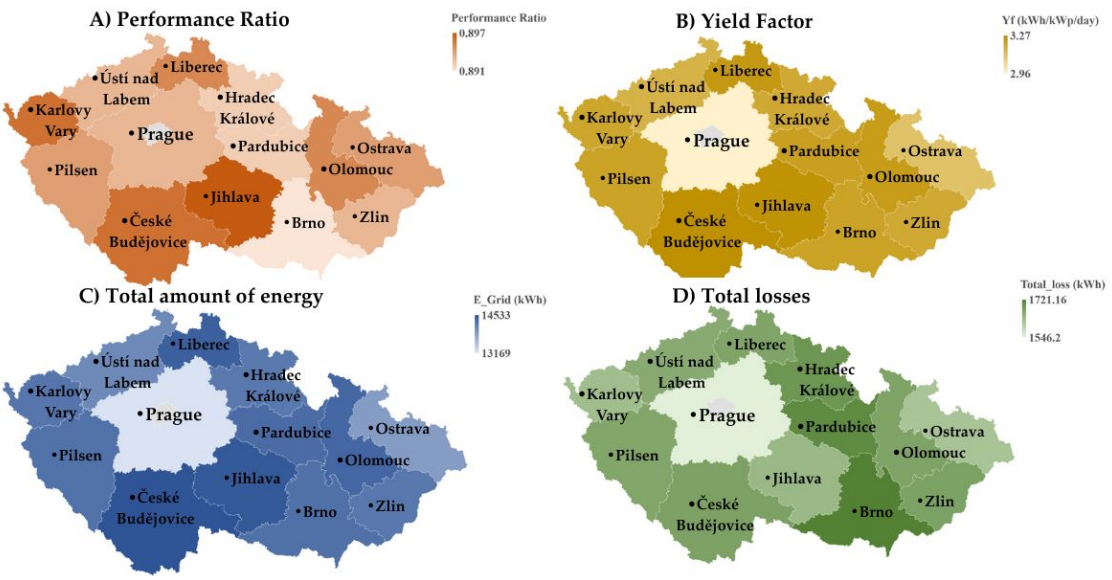

Figure Results and Discussion.11. Spatial distribution of annual PV performance across the Czech Republic: (A) Performance Ratio PR (%), (B) final yield Y_f (kWh/kWp/day), (C) energy injected to grid E_{Grid} (kWh/year), (D) total system losses (kWh/year). Interpolated using inverse distance weighting from 13 province data points.

Figure 4.9A shows PR varying from 89.1% (Brno) to 89.7% (Jihlava), with the highest efficiency concentrated at higher-altitude inland provinces and in the western region (Karlovy Vary, Plzen). The spatial gradient reflects the altitude-temperature-PR interaction: Jihlava benefits from its 524 m elevation to maintain lower ambient temperatures and superior thermal efficiency, confirming that altitude is a moderating variable not captured by latitude alone [39].

Figure 4.9B shows Y_f highest in the south and southeast (Ceske Budejovice 3.27, Jihlava 3.24, Plzen 3.22 kWh/kWp/day) and lowest in the northwest and capital (Prague 2.96, Usti nad Labem 3.05 kWh/kWp/day). The 10.5% difference between the best and worst province represents the maximum attainable improvement from site selection alone within the Czech Republic. Expressed in nZEB terms, E_{grid} from Ceske Budejovice (14,533 kWh/year, Figure 4.9C) covers approximately 48-58% of total primary energy consumption of a typical Czech single-family house (100 m^2, 90-130 kWh/m^2/year), while Prague (13,169 kWh/year) covers 40-53% - an 8-12 percentage point coverage gap with direct implications for ZEB compliance under Directive 2024/1275/EU [3].

Figure 4.9D shows total losses peaking in the south (Brno 1,721.2 kWh/year) where higher irradiance drives larger absolute thermal and mismatch losses, while central regions including Prague experience lower absolute losses. As discussed in Section 4.5, this apparent paradox - Prague lowest losses yet lowest yield - is resolved by recognizing that losses scale with throughput; the PR (Figure 4.9A) correctly normalizes for this effect.

Comparing to similar nationwide studies: Malvoni et al. [42] documented larger performance gradients across Italy (PR 78-83%, Y_f 3.8-5.2 kWh/kWp/day) due to the pronounced latitudinal irradiance gradient between Alpine and Mediterranean climates. The Czech Republic's narrower range confirms that its compact C_{fb}/D_{fb} climate limits spatial differentiation, but the 10.5% Y_f variation still represents a meaningful design variable for provincial-level building energy policy.

4.8 Multivariate Statistical Analysis

Figure 4.10 presents the full multivariate statistical analysis suite applied to the province performance dataset.

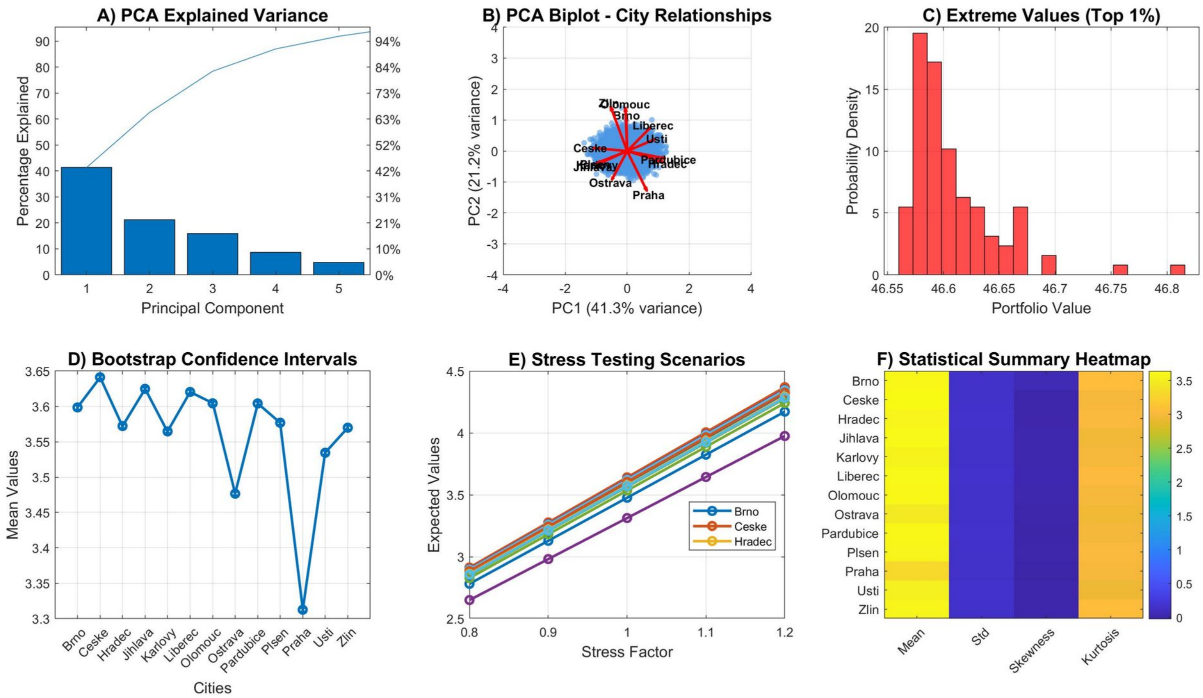

Figure Results and Discussion.12. Multivariate statistical analysis: (A) PCA scree plot - explained variance per principal component, (B) PCA biplot - province scores in PC1-PC2 space with variable loadings, (C) extreme value distribution (top 1% of Monte Carlo outputs), (D) bootstrap confidence intervals for mean Y_f per province, (E) stress testing scenarios showing expected Y_f per province scaled across a range of stress factors (0.8-1.2), (F) statistical summary heatmap (mean, standard deviation, skewness, kurtosis).

4.8.1 Principal Component Analysis

Figure 4.10A shows that PC1 and PC2 explain 41.3% and 21.2% of total variance respectively, jointly accounting for 62.5%, with a third component contributing a further 16.0%. While the first two components remain the dominant drivers, the more gradual decline in explained variance across components indicates a less sharply two-dimensional structure than a single dominant pair would suggest [27]. PC1 represents a solar resource intensity axis: provinces loading positively (Ceske Budejovice, Jihlava, Plzen) are characterized by higher annual GHI and Y_f; those loading negatively (Prague, Usti nad Labem) are characterized by lower resource quality. PC2 represents a thermal efficiency axis: positively loading provinces (Jihlava, Karlovy Vary) exhibit lower ambient temperatures and higher PR; negatively loading provinces (Brno) experience higher temperatures and higher total losses.

Figure 4.10B (PCA biplot) shows that Olomouc, Brno, and Zlin cluster together along the positive PC2 direction, while Ostrava and Praha cluster at the opposite, negative end of the same axis - separating provinces by thermal/efficiency profile as PC2 was defined to do. Along a second direction, Pardubice and Hradec Kralove cluster together, distinct from Liberec and Usti nad Labem, while Ceske Budejovice, Karlovy Vary, Jihlava, and Plzen form a fourth, more central grouping. This five-way structure is less cleanly separable into two opposing clusters than the earlier two-component reading suggested, consistent with the additional variance now carried by the third principal component.

4.8.2 Extreme Values and Bootstrap Intervals

Figure 4.10C examines the extreme value distribution (top 1% of Monte Carlo realizations), concentrated in the portfolio value range of 46.55-46.8 normalized units - a narrow band reflecting that provincial variability is only partially correlated, so extreme portfolio-wide outcomes require simultaneous, aligned deviations across many provinces rather than a single dominant common factor. These rare, high-output scenarios represent conditions of sustained above-average irradiance combined with below-average temperatures - plausible but infrequent climatic configurations. For grid planning, these tail scenarios set the upper bound on residential PV injection peaks, informing network capacity requirements [26].

Figure 4.10D presents bootstrap confidence intervals for mean Y_f per province (1,000 bootstrap resamples). Most provinces converge in the 3.55-3.65 range. Usti nad Labem and Ostrava fall toward the lower edge of this cluster (3.49–3.53), while Prague is a marked outlier at 3.31 - well below every other province - consistent with its comparatively poor tilt-latitude [27].

4.8.3 Stress Testing and Distributional Summary

Figure 4.10E (stress testing scenarios) shows each province's expected Y_f scaled uniformly across a range of stress factors from 0.8 to 1.2, representing hypothetical system-wide performance shifts such as long-term degradation, soiling, or measurement bias. Because the scaling is applied uniformly across all inputs, each province's response is linear and the relative ranking established in Table 2 is preserved across the full stress range - Praha remains the lowest-performing province at every stress level, while higher-yield provinces maintain a proportional lead throughout. This panel therefore illustrates the robustness of the relative provincial ranking to uniform system-wide shifts, rather than adding new comparative information beyond Table 2. Figure 4.10F (statistical heatmap) shows stable means across provinces but elevated kurtosis values for Ceske Budejovice and Jihlava, signaling heavy-tailed output distributions - a risk characteristic that is invisible in mean-based performance metrics but captured by the Monte Carlo ensemble.

K-means clustering ($k = 3$) on standardized PR, Total Losses, and Y_f (E_{grid} excluded as redundant with Y_f, $r = 0.9993$) produces a markedly asymmetric partition: a broad group of 7 provinces (Ostrava, Usti nad Labem, Hradec Kralove, Zlin, Plzen, Brno, Pardubice; mean $Y_f = 3.18$ kWh/kWp/day), a smaller higher-performing group of 5 provinces (Karlovy Vary, Olomouc, Liberec, Jihlava, Ceske Budejovice; mean $Y_f = 3.24$ kWh/kWp/day), and Prague as a singular, isolated cluster ($Y_f = 2.96$ kWh/kWp/day). The hierarchical dendrogram confirms this structure directly: the two larger groups merge into a combined branch at a moderate linkage height, while Prague joins the tree only at the final merge - the most isolated province by a wide margin, not part of a broader "low-performing region." The two non-Prague clusters differ from each other by only 1.7% in mean Y_f, indicating that provincial performance is fairly homogeneous across most of the Czech Republic; Prague is the outlier requiring distinct explanation, driven by its urban microclimate and comparatively poor tilt-latitude match (Section 4.1), not evidence of a broader multi-province regional divide.

4.8.4 Policy Implications of the Clustering Analysis

These clusters provide a directly actionable framework for region-differentiated building energy policy, though the actionable distinction is narrower than a three-region split would suggest: the higher-performing 5-province group, where 12 kWp rooftop systems most closely approach the nZEB energy offset threshold, could qualify for streamlined permitting and standard subsidy treatment, alongside the broader 7-province group whose performance differs only marginally. Prague, where the same system falls furthest short of the nZEB threshold, requires supplementary instruments - enhanced subsidies, mandatory building energy efficiency improvements, or community energy schemes - targeted specifically at the capital rather than a wider region [3], [9].

The technical performance differentiation intersects with social dimensions identified in the literature. Makesova et al. [9] found that financial subsidies are the dominant motivation for household PV adoption, cited by 83% of respondents, while 61% cited environmental benefits. If subsidy rates are nationally uniform - as under the current New Green Savings Program - households in Prague receive equal financial support despite systematically lower yields, creating an implicit cross-subsidy from Prague to the rest of the country that is not currently captured in the uniform national subsidy structure. Framing this two ways clarifies the policy picture. First, the general regional spread: the two non-Prague clusters differ by only 1.7% in mean Y_f (3.24 vs. 3.18 kWh/kWp/day), corresponding to a modest ~249 kWh/yr energy difference, ~1,370 CZK/yr, and an NPV difference of roughly 24,000 CZK over 25 years - small enough that a uniform national subsidy is broadly defensible across these 12 provinces. Second, Prague's distinct shortfall: at Y_f = 2.96 kWh/kWp/day, Prague underproduces the two clusters by 7.6% and 9.5% respectively, corresponding to an annual energy shortfall of approximately 1,000-1,250 kWh, a financial gap of roughly 5,500-6,850 CZK/year at the Czech 2025 household tariff of 5.5 CZK/kWh [45], [46], and a net present value disadvantage of approximately 95,000-119,000 CZK over a 25-year system lifetime at a 3% discount rate. This is a larger gap than previously estimated, because it now isolates Prague specifically rather than averaging it together with Usti nad Labem and Ostrava, which the corrected clustering shows do not share Prague's performance profile. This is an illustrative order-of-magnitude estimate rather than a formal techno-economic analysis. A region-differentiated subsidy mechanism calibrated to this gap would more equitably distribute the financial burden of nZEB compliance and could be incorporated within the existing New Green Savings Program administrative framework without requiring new legislative instruments. Tanil and Jurek's [8] finding that Czech renewable energy policy is driven primarily by EU compliance rather than domestic political ownership indicates a structural institutional vulnerability that the present technical findings cannot resolve but can contextualize: the provinces most exposed to performance uncertainty (Hradec Kralove, Usti nad Labem, Jihlava, Section 4.6) are precisely those where resilience to policy change matters most. Dzikuc et al. [44] identified outdated grid infrastructure and regulatory instability as binding constraints on PV integration in the Czech Republic and Poland. The portfolio analysis in Section 4.6 demonstrates that geographic diversification of residential PV reduces aggregate output variability, directly reducing the grid management challenge - an argument for policy that incentivizes deployment broadly across all provinces rather than concentrating in the higher-performing 5-province group, with particular attention to Prague given its distinct underperformance.

Gurtler et al.'s [47] study of PV policy dismantling in Spain and the Czech Republic showed that inflexible feed-in tariff designs create political backlash when deployment accelerates unexpectedly. The technically grounded, province-specific performance dataset presented in this thesis provides the evidential basis for an adaptive, performance-differentiated support mechanism resistant to the dismantling dynamics they describe.

Chapter 5: Conclusions and Future Work

5.1 Summary of Findings

This thesis conducted a systematic, multi-province performance evaluation of a standardized 12 kWp grid-connected rooftop PV system across all 13 administrative provinces of the Czech Republic, integrating deterministic PVsyst simulation, Monte Carlo uncertainty quantification, and multivariate statistical analysis. The study addresses three research gaps identified in Chapter 1: the absence of province-level PV performance benchmarks in the Czech Republic, the lack of probabilistic uncertainty characterization for Central European residential PV, and the absence of spatially resolved cluster analysis to support region-differentiated policy.

The five research objectives stated in Section 1.4 have been addressed as follows.

Objective 1: Provincial performance evaluation. The annual final yield (Y_f) ranges from 2.96 kWh/kWp/day in Prague to 3.27 kWh/kWp/day in Ceske Budejovice, representing a 10.5% difference attributable entirely to climatic and geographic factors rather than system design. The performance ratio (PR) varies narrowly from 89.1% (Brno) to 89.7% (Jihlava), among the highest values reported internationally for grid-connected residential systems, confirming that Central European temperate climates are exceptionally favorable for PV efficiency. Total annual energy delivered to the grid (E_{grid}) ranges from 13,169 kWh (Prague) to 14,533 kWh (Ceske Budejovice). All metrics are defined and reported in strict accordance with IEC 61724-1:2017.

Objective 2: Optimal tilt angle determination. The province-specific optimal tilt ranges from 38 to 42 degrees, systematically 8–12 degrees below the geographic latitude of 49–51 degrees N, with Prague showing the largest deviation (~12°) due to its comparatively low optimal tilt of 38° relative to its 50.1°N latitude. This deviation, explained by the high diffuse radiation fraction and summer-dominant energy balance of Czech C_{fb}/D_{fb} climates, has a design implication: applying the standard latitude rule in Czech residential construction would overestimate the optimal tilt and impose unnecessary energy losses. Seasonal analysis reveals that a fixed tilt at the annual optimum incurs up to 3% summer and 13% winter sub-optimality losses relative to the seasonal optima, quantifying the design trade-off inherent in fixed-tilt residential installations.

Objective 3: Monte Carlo uncertainty quantification. The Monte Carlo ensemble (N = 1000 per province) establishes that plane-of-array irradiance is the dominant uncertainty driver (sensitivity index 0.85-0.95), followed by ambient temperature (0.20-0.35) and module efficiency (0.15-0.25). System design parameters - inverter efficiency, soiling, ohmic losses - contribute sensitivity indices below 0.10, confirming that meteorological uncertainty is the primary source of performance risk and cannot be managed through system component selection alone. Hradec Kralove, Usti nad Labem, and Jihlava are identified as the highest-sensitivity provinces; Prague exhibits the most stable performance profile with the lowest Value-at-Risk at the 5% quantile.

Objective 4: Spatial and multivariate statistical analysis. PCA reduces the six-variable provincial performance matrix to two dominant components explaining 62.5% of total variance: a solar resource intensity axis (PC1, 41.3%) and a thermal efficiency axis (PC2, 21.2%), with a third component contributing an additional 16.0%. K-means clustering reveals a markedly asymmetric structure - two broadly comparable province groups (a 5-province higher-performing group and a 7-province group, differing by only 1.7% in mean Y_f) and Prague as a singular, isolated outlier (Y_f = 2.96 kWh/kWp/day, 7.6-9.5% below both groups) - providing the first data-driven provincial clustering of Czech PV performance in the literature, and identifying Prague specifically, rather than a broader region, as the primary driver of provincial performance disparity. The aggregate portfolio of 13 provinces exhibits a coefficient of variation (2.8%) lower than the mean provincial CV (4.3-4.5%), demonstrating the systemic risk-reduction benefit of geographic diversification.

Objective 5: Policy contextualization. The annual E_{grid} of 13,169-14,533 kWh corresponds to a nZEB coverage of 40-58% of the primary energy consumption of a typical Czech single-family house under the ZEB requirements of Directive 2024/1275/EU. This province-specific coverage differential - invisible in national-average analyses - constitutes a quantitative argument for region-differentiated subsidy design, supplementary energy efficiency requirements, and performance-calibrated permitting frameworks, particularly for Prague, where coverage falls furthest short of the threshold.

5.2 Critical Reflection on Limitations

Three limitations of the present study require explicit acknowledgement, as they define the boundary conditions within which the findings should be applied.

First, all simulations use synthetic typical meteorological year (TMY) data from Meteonorm 8.1 rather than multi-year measured irradiance records. TMY data represent long-term average conditions and do not capture inter-annual climate variability. The Monte Carlo framework partially addresses this limitation by treating irradiance as a stochastic variable with a 5% coefficient of variation, but this parameterization is itself derived from Meteonorm uncertainty estimates rather than from a measured inter-annual irradiance dataset for Czech provinces. Future work using measured multi-year irradiance records from ground stations or satellite-derived time series (e.g. PVGIS SARAH-2 hourly data) would provide a more robust empirical basis for the uncertainty bounds.

Second, near-shading from surrounding structures, vegetation, and rooftop obstructions is set to zero throughout. Real residential installations in urban environments - particularly in Prague and Ostrava, where building density is highest - will experience shading losses beyond those captured in the model. The Prague urban irradiance deficit documented in Chapter 4 is partly attributable to atmospheric effects (aerosol, fog), but building shading is an additional unquantified factor. Three-dimensional shading analysis using LiDAR-derived building geometry would be required to separate these effects and provide installation-specific yield estimates for urban settings.

Third, no formal techno-economic analysis is conducted. The study quantifies energy yield and system losses but does not compute a levelized cost of energy (LCOE) or simple payback period across provinces. An illustrative order-of-magnitude net present value gap between performance clusters is estimated in Chapter 4 (Discussion) using a fixed electricity tariff and discount rate, but this falls short of a full techno-economic analysis incorporating province-specific tariffs, subsidy structures, and financing assumptions, which are outside the defined scope. A companion economic analysis using the performance data generated here as input is recommended as an immediate priority for future work.

5.3 Recommendations for Future Research

Building on the limitations identified above and the findings of Chapter 4, the following research directions are recommended.

Techno-economic and life-cycle assessment. A comprehensive analysis combining the province-specific E_{grid} values from this study with Czech household electricity tariffs, subsidy structures under the New Green Savings Program, module degradation rates, and end-of-life recycling costs would produce LCOE and NPV estimates for each province cluster. This would directly translate the technical performance differentials into investment decision support, addressing the primary motivation of Czech residential PV adopters identified by Makesova et al [9].

Real-world 3D shading and building integration analysis. Extending the simulation framework to incorporate actual building geometry using LiDAR point cloud data for representative Czech residential typologies would quantify the shading penalty in urban versus rural settings. Combined with the provincial cluster analysis from this thesis, this would produce installation-specific yield maps at the neighborhood scale, supporting building permit applications and urban energy planning.

Dynamic system design with consumption profile matching. The present study evaluates system performance independently of building energy demand. Integrating hourly consumption profiles - differentiated by building type, occupancy pattern, and province - would enable self-consumption ratio analysis, battery sizing optimization, and the quantification of how much of the nZEB energy balance can be achieved through PV generation alone versus requiring additional efficiency measures. This is the natural next step toward full building energy simulation.

Multi-year climate variability analysis. Replacing the TMY meteorological input with 10-20 years of measured or satellite-derived hourly irradiance records would provide empirically grounded P50 and P90 yield estimates for each province, replacing the Monte Carlo-derived bounds used here. This is a prerequisite for bankable yield assessment and for quantifying how climate change projections - which show increasing summer temperatures and shifting precipitation patterns in Central Europe - will affect long-term residential PV performance in the Czech Republic.

Bifacial module and tracking system performance. The present study is limited to monofacial fixed-tilt modules. Analysis of bifacial N-type TOPCon modules - which capture ground-reflected albedo on the rear surface - would be particularly relevant for the high-albedo provinces identified in Chapter 4 (Hradec Kralove, Jihlava), where rear-side gains could meaningfully improve annual yield. Single-axis tracking systems, while uncommon in residential rooftop applications, are increasingly considered for larger building-integrated systems and community solar installations.

5.4 Concluding Statement

This thesis delivers, to the authors' knowledge, the first systematic, province-resolved, probabilistically bounded performance benchmark for residential grid-connected PV systems across the Czech Republic. The 10.5% spatial variation in final yield, the identification of three distinct province performance clusters, and the demonstration that irradiance uncertainty dominates system performance risk together constitute a technically rigorous foundation for evidence-based nZEB building design and region-differentiated renewable energy policy in the Czech Republic and, by extension, in comparable Central European building contexts. The findings confirm that temperate continental climates - long regarded as marginal for solar energy - are in fact among the most efficient environments for residential PV operation when system design is correctly optimized for local conditions.

Data Availability Statement

The simulation data, Monte Carlo analysis code, and statistical/clustering analysis code supporting this thesis are openly available on Zenodo at:
https://doi.org/10.5281/zenodo.21245813 [48], under a CC-BY 4.0 license.

References

[1] G. Masson, E. Bosch, A. Van Rechem, and M. De l'Epine, "Snapshot 2024," IEA Photovoltaic Power Systems Programme (PVPS), 2024. doi: 10.69766/VHRF4040.

[2] International Energy Agency (IEA), "Renewables 2025," International Energy Agency (IEA), Paris, 2025. [Online]. Available: https://www.iea.org/reports/renewables-2025

[3] European Parliament and Council, "Directive (EU) 2024/1275 of 24 April 2024 on the energy performance of buildings (recast)," *Off. J. Eur. Union*, vol. OJ L, May 2024, [Online]. Available: https://eur-lex.europa.eu/eli/dir/2024/1275/oj

[4] K. Bódis, I. Kougias, A. Jäger-Waldau, N. Taylor, and S. Szabó, "A high-resolution geospatial assessment of the rooftop solar photovoltaic potential in the European Union," *Renew. Sustain. Energy Rev.*, vol. 114, p. 109309, Oct. 2019, doi: 10.1016/j.rser.2019.109309.

[5] G. Osma-Pinto and G. Ordóñez-Plata, "Measuring factors influencing performance of rooftop PV panels in warm tropical climates," *Sol. Energy*, vol. 185, pp. 112–123, Jun. 2019, doi: 10.1016/j.solener.2019.04.053.

[6] "Úvod," Solární asociace. Accessed: May 28, 2026. [Online]. Available: https://solarniasociace.cz/

[7] "Free Solar Maps & GIS Data | High-Res Download | Solargis." Accessed: May 28, 2026. [Online]. Available: https://solargis.com/resources/free-maps-and-gis-data?locality=czech-republic

[8] G. Tanil and P. Jurek, "Policies on renewable energy at the European and national level of governance: Assessing policy adaptation in the Czech Republic," *Energy Rep.*, vol. 6, pp. 548–553, Feb. 2020, doi: 10.1016/j.egyr.2019.09.024.

[9] M. Makešová, M. Valentová, and M. Pilnáček, "Motivation for households' investment in photovoltaics in Czechia: An exploratory factor analysis," *Energy Res. Soc. Sci.*, vol. 106, p. 103262, Dec. 2023, doi: 10.1016/j.erss.2023.103262.

[10] A. Mermoud and T. Lejeune, "Performance Assessment of a Simulation Model for PV Modules of Any Available Technology," *25th Eur. Photovolt. Sol. Energy Conf. Exhib. 5th World Conf. Photovolt. Energy Convers.*, vol. 6-10 September 2010, p. 6 pages, 3678 kb, 2010, doi: 10.4229/25THEUPVSEC2010-4BV.1.114.

[11] N. Riedel-Lyngskær *et al.*, "Validation of Bifacial Photovoltaic Simulation Software against Monitoring Data from Large-Scale Single-Axis Trackers and Fixed Tilt Systems in Denmark," *Appl. Sci.*, vol. 10, no. 23, p. 8487, Nov. 2020, doi: 10.3390/app10238487.

[12] International Electrotechnical Commission, "IEC 61724-1:2017," no. Photovoltaic system performance-Part 1: Monitoring, Mar. 2017, [Online]. Available: https://webstore.iec.ch/en/publication/33622

[13] A. Saltelli *et al.*, *Global Sensitivity Analysis. The Primer*, 1st ed. Wiley, 2007. doi: 10.1002/9780470725184.

[14] F. F. Ahmad, M. Abdelsalam, A. K. Hamid, C. Ghenai, W. Obaid, and M. Bettayeb, "Experimental Validation of PVSYST Simulation for Fix Oriented and Azimuth Tracking Solar PV System," in *Modelling, Simulation and Intelligent Computing*, vol. 659, N. Goel, S. Hasan, and V. Kalaichelvi, Eds., in Lecture Notes in Electrical Engineering, vol. 659. , Singapore: Springer Singapore, 2020, pp. 227–235. doi: 10.1007/978-981-15-4775-1_25.

[15] M. E. Becquerel, "Mémoire sur les effets électriques produits sous l'influence des rayons solaires," *Comptes Rendus Hebd. Séances Académie Sci.*, vol. 9, pp. 561–567, 1839.

[16] A. Einstein, "On a heuristic point of view concerning the production and transformation of light," *Ann. Phys.*, pp. 1–18, 1905.

[17] S. M. Sze, Y. Li, and K. K. Ng, *Physics of semiconductor devices*. John wiley & sons, 2021.
[18] W. Shockley, “The Theory of *p-n* Junctions in Semiconductors and *p-n* Junction Transistors,” *Bell Syst. Tech. J.*, vol. 28, no. 3, pp. 435–489, Jul. 1949, doi: 10.1002/j.1538-7305.1949.tb03645.x.
[19] J. A. Duffie and W. A. Beckman, *Solar Engineering of Thermal Processes*, 1st ed. Wiley, 2013. doi: 10.1002/9781118671603.
[20] A. Luque and S. Hegedus, Eds., *Handbook of Photovoltaic Science and Engineering*, 1st ed. Wiley, 2010. doi: 10.1002/9780470974704.
[21] D. L. King, J. A. Kratochvil, and W. E. Boyson, *Photovoltaic array performance model*, vol. 8. United States. Department of Energy, 2004.
[22] E. Karatepe, M. Boztepe, and M. Çolak, “Development of a suitable model for characterizing photovoltaic arrays with shaded solar cells,” *Sol. Energy*, vol. 81, no. 8, pp. 977–992, Aug. 2007, doi: 10.1016/j.solener.2006.12.001.
[23] A. D. Dhass, N. Beemkumar, S. Harikrishnan, and H. M. Ali, “A Review on Factors Influencing the Mismatch Losses in Solar Photovoltaic System,” *Int. J. Photoenergy*, vol. 2022, pp. 1–27, Feb. 2022, doi: 10.1155/2022/2986004.
[24] A. J. Marszal *et al.*, “Zero Energy Building – A review of definitions and calculation methodologies,” *Energy Build.*, vol. 43, no. 4, pp. 971–979, Apr. 2011, doi: 10.1016/j.enbuild.2010.12.022.
[25] M. Vins and M. Gangur, “SIMPLIFIED METHODOLOGY OF ECONOMIC EVALUATION OF HOUSEHOLD PV INSTALLATIONS IN CZECH REPUBLIC USING MONTE CARLO METHOD,” *Adv. Electr. Electron. Eng.*, vol. 22, no. 4, pp. 345–355, Dec. 2024, doi: 10.15598/aeee.v22i4.240406.
[26] L.-F. Duque, E. O’Connell, and G. O’Donnell, “A Monte Carlo simulation and sensitivity analysis framework demonstrating the advantages of probabilistic forecasting over deterministic forecasting in terms of flood warning reliability,” *J. Hydrol.*, vol. 619, p. 129340, Apr. 2023, doi: 10.1016/j.jhydrol.2023.129340.
[27] I. T. Jolliffe, *Principal Component Analysis*. in Springer Series in Statistics. New York: Springer-Verlag, 2002. doi: 10.1007/b98835.
[28] “Global Solar Data | Meteonorm.” Accessed: May 31, 2026. [Online]. Available: https://meteonorm.com/
[29] “Optimization tools - PVsyst documentation.” Accessed: Apr. 14, 2025. [Online]. Available: https://www.pvsyst.com/help/project-design/orientations-in-v8/optimization-tools.html
[30] “Jinko Solar Energy Kits.” Accessed: May 31, 2026. [Online]. Available: http://www.jinkopvsolar.com/JINKO.html
[31] Huawei Technologies Co., Ltd, “SUN2000-8/10/12/15/17/20KTL-M2 Datasheet,” Huawei Digital Power. Accessed: Jul. 06, 2026. [Online]. Available: https://solar.huawei.com/-/media/Solar/attachment/pdf/apac/datasheet/SUN2000-12-20KTL-M2.pdf
[32] “IEC 62548:2016.” Accessed: May 31, 2026. [Online]. Available: https://webstore.iec.ch/en/publication/25949
[33] “PVsyst documentation.” Accessed: May 31, 2026. [Online]. Available: https://www.pvsyst.com/help/
[34] A. Mermoud and B. Wittmer, “PVSYST USER’S MANUAL”.
[35] W. Diao, Y. Zhao, Y. Dong, J. Zhai, Q. Wang, and Y. Gui, “Spatiotemporal Variability of Surface Wind Speed during 1961–2017 in the Jing-Jin-Ji Region, China,” *J. Meteorol. Res.*, vol. 34, no. 3, pp. 621–632, Jun. 2020, doi: 10.1007/s13351-020-9119-5.

[36] J. Antonanzas, R. Urraca, F. J. Martinez-de-Pison, and F. Antonanzas, “Optimal solar tracking strategy to increase irradiance in the plane of array under cloudy conditions: A study across Europe,” *Sol. Energy*, vol. 163, pp. 122–130, Mar. 2018, doi: 10.1016/j.solener.2018.01.080.
[37] A. A. Stephen, K. Musasa, and I. E. Davidson, “Modelling of Solar PV under Varying Condition with an Improved Incremental Conductance and Integral Regulator,” *Energies*, vol. 15, no. 7, p. 2405, Mar. 2022, doi: 10.3390/en15072405.
[38] V. Sharma and S. S. Chandel, “Performance analysis of a 190 kWp grid interactive solar photovoltaic power plant in India,” *Energy*, vol. 55, pp. 476–485, Jun. 2013, doi: 10.1016/j.energy.2013.03.075.
[39] N. M. Kumar, R. P. Gupta, M. Mathew, A. Jayakumar, and N. K. Singh, “Performance, energy loss, and degradation prediction of roof-integrated crystalline solar PV system installed in Northern India,” *Case Stud. Therm. Eng.*, vol. 13, p. 100409, Mar. 2019, doi: 10.1016/j.csite.2019.100409.
[40] R. W. Andrews and J. M. Pearce, “The effect of spectral albedo on amorphous silicon and crystalline silicon solar photovoltaic device performance,” *Sol. Energy*, vol. 91, pp. 233–241, May 2013, doi: 10.1016/j.solener.2013.01.030.
[41] N. Sahouane *et al.*, “Energy and economic efficiency performance assessment of a 28 kWp photovoltaic grid-connected system under desertic weather conditions in Algerian Sahara,” *Renew. Energy*, vol. 143, pp. 1318–1330, Dec. 2019, doi: 10.1016/j.renene.2019.05.086.
[42] M. Malvoni, A. Leggieri, G. Maggiotto, P. M. Congedo, and M. G. De Giorgi, “Long term performance, losses and efficiency analysis of a 960 kW P photovoltaic system in the Mediterranean climate,” *Energy Convers. Manag.*, vol. 145, pp. 169–181, Aug. 2017, doi: 10.1016/j.enconman.2017.04.075.
[43] I. Čábelková, W. Strielkowski, I. Firsova, and M. Korovushkina, “Public Acceptance of Renewable Energy Sources: a Case Study from the Czech Republic,” *Energies*, vol. 13, no. 7, p. 1742, Apr. 2020, doi: 10.3390/en13071742.
[44] M. Dzikuć, A. Piwowar, and M. Dzikuć, “The Development of Photovoltaics in the Countries of Central and Eastern Europe in the Context of Regulatory Changes: A Case Study of the Czech Republic and Poland,” *Energies*, vol. 18, no. 4, p. 817, Feb. 2025, doi: 10.3390/en18040817.
[45] “Household electricity prices in 1st half of 2025: -0.5%.” Accessed: Jun. 09, 2026. [Online]. Available: https://ec.europa.eu/eurostat/web/products-eurostat-news/w/ddn-20251029-2
[46] “Czechia: household electricity prices 2025,” Statista. Accessed: Jun. 09, 2026. [Online]. Available: https://www.statista.com/statistics/418073/electricity-prices-for-households-in-the-czech-republic/?utm_source=chatgpt.com
[47] K. Gürtler, R. Postpischil, and R. Quitzow, “The dismantling of renewable energy policies: The cases of Spain and the Czech Republic,” *Energy Policy*, vol. 133, p. 110881, Oct. 2019, doi: 10.1016/j.enpol.2019.110881.
[48] A. Ahmadi, “Simulation, Monte Carlo, and Statistical Analysis Data and Code — Grid-Connected PV Performance Across 13 Czech Provinces.” Zenodo, Jul. 07, 2026. doi: 10.5281/ZENODO.21245813.